CHAPTER

10

Using UAV and LiDAR data for gully geomorphic changes monitoring

Mihai Niculiță[a], *Mihai Ciprian Mărgărint*[a], *Paolo Tarolli*[b]

[a]Department of Geography, Faculty of Geography and Geology, Alexandru Ioan Cuza University of Iași, Iași, Romania [b]Department of Land, Environment, Agriculture and Forestry, University of Padova, Legnaro, Padova, Italy

OUTLINE

1 Introduction

A detailed knowledge of landform topography allows us varied and complex geomorphometric characterization, computation of different indices, and also offers an enriched perspective on the history and processes that shaped the Earth's surface (Tarolli et al., 2019a). The large variety of new technologies used in geomorphology changed the face

of this science (Inkpen, 2018), by shifts registered in the transition from poor to rich data, from field analysis to modeled reality and local surveys (Piegay et al., 2015), from analogue to digital technologies, and the miniaturization and portability which changed the nature and the quantities of data recorded in the field (Viles, 2016). Among these technologies, airborne and terrestrial LiDAR (light detecting and ranging), digital photogrammetry, and structure from motion (SfM) provide a large spectrum of data in order to obtain accurate and low-cost digital elevation models (DEMs). Due to their submeter resolution and the relatively high accuracy, the applications of these technologies are widespread in the analysis of many landforms which are characterized by fine fingerprints and whose evolution involved gradual processes (Tarolli, 2014; Passalacqua et al., 2015). This is the case of gully erosion which shows large year-to-year variation (Vanmaercke et al., 2016) and involves various processes (head retreat, bank retreat, scour, bank landslides, deposition) that create a complex and fine morphology, which can be depicted on high-resolution DEMs.

Gully erosion is recognized not only as an important process of soil erosion and a source of sediments (Poesen et al., 1996, 1998, 2003, 2006; Nagasaka et al., 2005), very often neglected in sediment budget studies, but also of environmental and land degradation and economic losses for agricultural lands (Poesen et al., 2003, 2006). Gully research is needed in order to fully conceptualize these complex phenomena that create gully landforms in order to establish clear measures that can diminish their effects on land degradation (Heede, 1976; Bocco, 1991; Poesen et al., 2006; Bergonse and Reis, 2011). Gully monitoring evolved from topographic mapping (Ireland et al., 1939; Leopold and Miller, 1956; Schumm and Hadley, 1957; Tuckfield, 1964), to photogrammetry (Giménez et al., 2009; Marzolff and Poesen, 2009) and remote sensing (Bocoo and Valenzuela, 1993). Currently, not many research studies fully exploited the use of LiDAR and low-cost SfM, in characterizing gullies and in the rate of process studies of gully erosion, with a few exceptions (Lannoeye et al., 2016; Gong et al., 2019). The studies dedicated to the usage of low-cost DEMs were mainly focused on small areas and on proof of concept regarding the workflow, errors, and gully features that can be modeled and mapped (Marzolff et al., 2011; Peter et al., 2014; Frankl et al., 2015; Stöcker et al., 2015; Liu et al., 2016; Glendell et al., 2017; Koci et al., 2017).

Our approach targets the usability of readily available datasets, such as LiDAR and low-cost technology, such as UAV SfM, coupled with DEM of Difference (DoD) analysis (Wheaton et al., 2010), to assess gully geomorphometry and rate of process.

1.1 LiDAR in geosciences

After experiments in the 1960s and 1970s, LiDAR acquiring topography technology became functional in the 1980s and 1990s, revolutionizing the elevation acquisition (Hickman and Hogg, 1969; Irish and White, 1998; Wehr and Lohr, 1999). In the 1990s and early 2000s, bathymetry and topography LiDAR systems were used to map from regional areas through airborne systems to solar system planets through satellite-borne systems (Smith et al., 1997, 1999). Nowadays, it is envisioned that, in the near future, large swaths of Earth will be covered with accessible LiDAR data, and the applications for the Earth's surface are very

diverse, becoming a de facto tool in geosciences (Harpold et al., 2015), including geoscience education (Robinson et al., 2017).

LiDAR high-resolution DEMs have been successfully used not only in landslide detection and mapping (McKean and Roering, 2004; Guzzetti et al., 2012; Tarolli et al., 2012; Lin et al., 2013; Niculiţă, 2016; Niculiţă et al., 2016) and in landslide dynamic and hazard assessment (Dewitte et al., 2008; Derron and Jaboyedoff, 2010; Schürch et al., 2011; Ventura et al., 2011; Jaboyedoff et al., 2012; Haas et al., 2012; Liu et al., 2018), but also in testing limits in landslide modeling (Penna et al., 2014). In fluvial geomorphology, the applications of LiDAR are various, from threshold mapping of channel network initiation (Tarolli and Dalla Fontana, 2009; Passalacqua et al., 2010; Orlandini et al., 2011), to morphology and dynamics of channel beds (Cavalli et al., 2008; Notebaert et al., 2009; Trevisani et al., 2010; Cavalli and Tarolli, 2011; Brasington et al., 2012; Javernick et al., 2014). LiDAR technologies have been used also in gully delineation and mapping (James et al., 2007; Momm et al., 2011, 2013; Wu et al., 2017; Xu et al., 2017) and the assessment of erosion rates (Evans and Lindsay, 2010; Perroy et al., 2010; Wang et al., 2016), or soil erosion (Eltner and Baumgart, 2015), both as TLS (terrestrial laser scanning) or as ALS (airborne laser scanning). Important results in the use of LiDAR were registered in the study of anthropic landforms such as mining activities, agricultural terraces, farmlands, and roads (Sofia et al., 2016; Tarolli and Sofia, 2016; Cao et al., 2020).

1.2 Digital photogrammetry and SfM in geosciences

After the emergence of low-cost computers and cameras, low-cost close range digital photogrammetry has become widely used to obtain high-resolution representations of the Earth's surface, where the elevation of the landforms is targeted (Barker et al., 1997; Aschenwald et al., 2001; Heimsath and Farid, 2002; Remondino and El-Hakim, 2006; Matthews, 2008; Fraser and Cronk, 2009; Eltner et al., 2016) in areas where dense vegetation is not present.

The structure-from-motion approach dates from back in the 1980s and is based on the work done in computer vision in order to reconstruct the 3D position of the camera based on the unconnected elements in motion (Ullman, 1979; Longuet-Higgins, 1981), which are recognized in multiple views. The scale invariant feature transform (SIFT) algorithm is used to find point features between every pair of images (Lowe, 1999, 2001, 2004). The RANSAC algorithm (Fischler and Bolles, 1981) estimates a fundamental matrix for every pair and creates connectivity graphs (Snavely et al., 2008). The estimation of camera parameters (rotation, translation, focal length, radial distortions) is done in an iterative way (Nistér, 2004; Snavely et al., 2008) in order to create the jointly optimal 3D structure through bundle adjustment (Triggs et al., 2000; Snavely et al., 2008). The final result consists of a sparse point cloud and reconstructed camera poses. Further, the sparse point cloud is used to obtain the densified point cloud, through depth map merging methods (Micusik and Kosecka, 2009; Li et al., 2010; Carrivick et al., 2016).

The developments of algorithms for image-based terrain extraction have made it possible to achieve good quality topographic data in terms of accuracy and precision from overlapping

stereo pairs from any angle (Chandler, 1999; Lane et al., 2000), through improvements of the methods to calibrate low-cost digital single lens reflex (DSLR) cameras (Clarke and Fryer, 1998; Chandler et al., 2005; Remondino and El-Hakim, 2006). In this way, any scientist can acquire good topographic data for small areas, with a wide range of uses in geomorphology. Further, the low-cost UAV that can support low-cost cameras (Giordan et al., 2018) extended the spatial range and the quality of the topography reconstructions, because spatial settings similar to and better than classic photogrammetry could be applied.

The application of digital photogrammetry and SfM techniques in geosciences (Westoby et al., 2012; Colomina and Molina, 2014; Carrivick et al., 2016) up to now includes various geomorphology fields such as: (i) laboratory-scale models of landscape evolution (Stojic et al., 1998; Hancock and Willgoose, 2001; Lane et al., 2001; Brasington and Smart, 2003; Rieke-Zapp and Nearing, 2005; Heng et al., 2010; Smith and Vericat, 2015; Momm et al., 2017); (ii) fluvial bed morphology (Heritage et al., 1999; Lane, 2000; Lane et al., 2000, 2001; Chandler et al., 2003; Brasington and Smart, 2003; Bird et al., 2010; Strick et al., 2019; Cucchiaro et al., 2018); (iii) riverbank erosion (Barker et al., 1997; Pyle et al., 1997; Prosdocimi et al., 2015; Hamshaw et al., 2017); (iv) soil erosion (Eltner et al., 2013, 2015, 2017; Hänsel et al., 2016; Prosdocimi et al., 2017; Di Stefano et al., 2019); (v) gully erosion (Betts and DeRose, 1999; Marzolff and Poesen, 2009; Gómez-Gutiérrez et al., 2014; Kaiser et al., 2014; Castillo et al., 2015, 2018; Frankl et al., 2015; Gesch et al., 2015; Stöcker et al., 2015; Vinci et al., 2015; Di Stefano et al., 2017; Glendell et al., 2017; Qin et al., 2019); (vi) glacier and proglacial surface change (Baltsavias et al., 2001; Keutterling and Thomas, 2006; Ely et al., 2016; Piermattei et al., 2016); (vii) geology mapping (Krosley et al., 2006; Sturznegger and Stead, 2009); (viii) rock slope stability analysis (Haneberg, 2008); (ix) landslide mapping and monitoring (Giordan et al., 2018; Peppa et al., 2018); (x) agriculture (Tarolli et al., 2019b); and (xi) anthropogenic landforms (Chen et al., 2015; Xiang et al., 2018; Pijl et al., 2020).

2 Study area: The reservoir bottom gullies from Jijia Hills (Romania)

The lowland of Northeastern Romania (Fig. 1) is well known for its reservoir construction history, sedimentation, and decommissioning during the last 500 years (Niculiță et al., 2017). These reservoirs were in general small (under 1 million m^3), shallow (4- to 8-m dam height with water depth of up to 5 m), and frequently dry during the summer or winter (Mărgărint and Niculiță, 2016; Niculiță et al., 2017; Mărgărint et al., 2017a,b). Their construction was requested by the dryness of the climate, the reservoirs being used for water storage, pisciculture, for cereals and fuller mills.

After reservoir filling, the dam topography remained and became smooth over time. The dams were cut in the principal spillway outlet area, in the auxiliary outlet area or in the median part of the dam, in order to evacuate/drain the groundwater, so that the reservoir bottom could be used as pasture. This anthropic intervention created a concentration of flow at high water discharges in the cut area, which allowed the evolution of gullies on the flat

lacustrine bottom. In other cases for the same effect of groundwater draining, linear channels were cut along the median line of the reservoir bottom. In these cases, bank gullies developed and evolved on the flat lacustrine bottom in areas where effluent discharge drained toward the anthropic channel. The reservoir sediments are predominantly silty, with layers of calcite duricrusts (Mărgărint et al., 2017a,b).

In the Jijia Hills of northeastern Romania, we identified 489 gullies, from which 68 showed changes in the aerial images from 2005 and 2010, and Google Earth high-resolution satellite imagery. From these 68 active gullies we have selected 4 gullies (Fig. 1) that were surveyed in the late winter and the early spring of 2019. Two of the gullies are located south of Săveni City (Botoşani County, Romania) in the Ghiţălăria catchment (20 km^2), tributary to the Sitna River, and the other two are located east of Şoldăneşti village (Botoşani County, Romania) in the Rogojeni catchment (61 km^2), tributary to the Jijia River. For simplicity's sake, the sites were labeled after the name of the locality and the upstream or downstream location in the catchment.

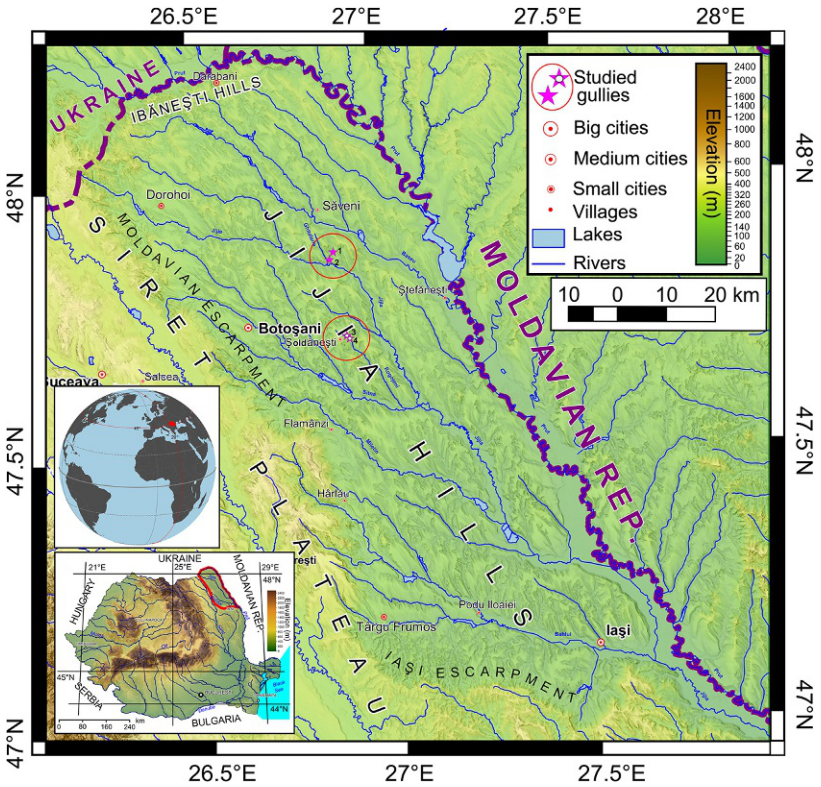

FIG. 1 Jijia Hills and the study cases: 1—Săveni upstream, 2—Săveni downstream, 3—Şoldăneşti upstream, 4—Şoldăneşti downstream.

3 Materials and methods

3.1 LiDAR data

LiDAR data were acquired at the end of 2012 with a Leica ALS60 system in geographic coordinates on the ETRS89 datum (EPSG:4258) by a company commissioned by the Prut-Bârlad Water Administration. The point clouds (.las format v 1.1) were classified with an unspecified algorithm and software to ASPRS 1.1 format classes. The point clouds for the entire project (21,708 km^2) were georeferenced using a network of 387 geodetic points, measured both in ERTS89 and Stereo 70 Marea Neagră datums and for which a quasi-geoid model was computed. The vertical accuracy (expressed as the root mean square area [RMSE] of elevation difference) is 0.19 m, in line with data used in the literature (Adams and Chandler, 2002; Bowen and Waltermire, 2002; Hodgson and Bresnahan, 2004).

We used GDAL and proj4 to convert between EPSG:4258 to EPSG:3844 horizontal datums. No vertical datum conversion was performed since GPS coordinates were acquired in ERTS89 through the https://www.rompos.ro differential correction service.

Because the algorithm of the point cloud classification is not known, and because through remote sensing investigation (aerial imagery draped over the DEM and 3D views with the point cloud) we observed that especially the landform edges (gully bank and other scarps) are not correctly located (due to low vegetation identification on these edges), we have chosen to process ourselves the point clouds for bare-earth extraction (Liu, 2008). The multiscale curvature classification (MCC) algorithm (Evans and Hudak, 2007) was used because the study area has a low tree cover and the low grassy vegetation can be easily depicted by the curvature parameter used by this algorithm, due to the fact that the data were acquired in midwinter, with low snow cover. Multiple runs with different parameters of the algorithm (scale parameters with values between 0.1 and 3 m and curvature parameter with values between 0.05 and 0.4) were assessed (Fig. 2—DEMs were derived from the TIN interpolation of the point clouds; the highlighted DEM represents the run from which the values of the parameters were chosen). As we increased the scale factor, more and more ground data were considered to have a low vegetation cover and, as a consequence, were removed. The most affected areas are located on the edges of the gully banks and other scarps. The question that arose is what is acceptable: to lose information about the erosional morphology or to remove the vegetation entirely. In our case, we argue that keeping the morphology is important, since vegetation can be later removed from the DTM through filtering, or even manually, or as in our case this is not so important because the gullies have important erosional surfaces, where very low vegetation cover occurs. Finally, we have chosen as parameters for the MCC algorithm a scale of 0.5 and curvature of 0.1. We strongly advise others to use their own assessment in order to select the right parameters, because our gullies are in their majority free of vegetation during late autumn and winter (grasses decay after the very dry late summer and early autumn), when both the LiDAR and UAV data were acquired.

The descriptions of the point cloud density and spacing before and after classification are reported in Table 1.

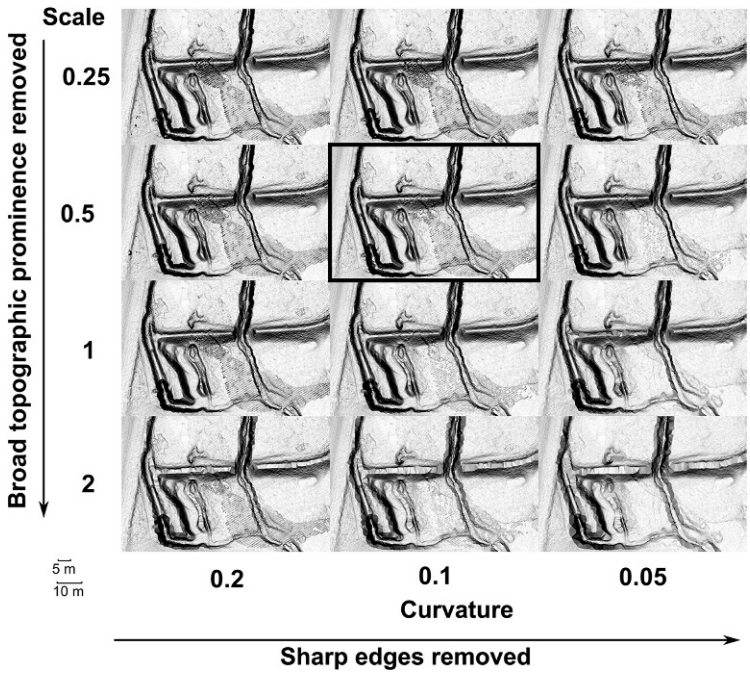

FIG. 2 Multiscale Curvature Classification (MCC) algorithm results and the chosen values (the corresponding image is *bolded*).

TABLE 1 The details of LiDAR data for the areas of each gully.

ID	Name	Flight date	Density (points/m^2)	Mean spacing (m)	Density of ground points (points/m^2)	Mean spacing of ground points (m)
1	Săveni downstream	01/21/2012	2.06	0.35	1.98	0.35
2	Săveni upstream	01/21/2012	3.68	0.26	3.68	0.26
3	Şoldăneşti downstream	01/21/2012	1.81	0.43	1.74	0.44
4	Şoldăneşti upstream	01/21/2012	1.16	0.81	1.16	0.81

3.2 UAV images

The Phantom 4 Pro quadcopter was used to capture the images in stereo pairs (models) as a string and block photogrammetric flight path (Falkner and Morgan, 2002; Linder, 2016) with the help of the PrecisionFlight pre-planning mobile application (https://www.precisionhawk.com/precisionflight). The altitude of the flight was 50 m relative to the takeoff location (close to the car that appears as reference in Figs. 9–12), and side and forward (end) overlap of 80% (Falkner and Morgan, 2002). The camera acquired images at 20 MP resolution, in 3:2 Aspect Ratio with a size of 5472 × 3648 pixels per image. The nominal pixel size was of

~0.01157 m. The characteristics of the Phantom 4 Pro camera are: FOV 84° 8.8 mm/24 mm (35 mm format equivalent) and $f/2.8$–$f/11$ auto focus at 1 m to ∞. Because the calibration parameters of the Phantom 4 Pro camera are not implemented in the utilized SfM software, the images were acquired in RAW format without geometric corrections of the software of the camera. The camera parameters were estimated by the SfM process. The ground control points were marked as targets in the field and measured using a Trimble R4 rover with the Rompos RTK correction (with centimetric accuracy, ±3 cm horizontal and ±6 cm vertical) in EPSG:3844 projection and ERTS89 vertical datum.

3.3 Structure from motion

3.3.1 SfM approach

The software used for the SfM technique was VisualSFM version 0.5.26 with the PMVS/CMVS tool chain (Wu et al., 2011; Wu, 2013, 2015; Shan et al., 2014; Zheng and Wu, 2015), which is free (http://ccwu.me/vsfm/). The software performs the classical SfM technique (Fig. 3) through: (i) pairwise image matching through an SIFT; (ii) followed by full pairwise image matching, sparse reconstruction of the point cloud based on the matched points between images with bundle adjustment (Snavely et al., 2006, 2008); (iii) GCPs identification and x,y,z setting for geometrical correction (scale and orientation) of the point cloud; and (iv) finally the dense reconstruction of the point cloud by clustering views for multi-view stereo (CMVS) and patch-based multi-view stereo (PMVS) algorithms (Furukawa and Ponce, 2007, 2010; Furukawa et al., 2010). Visual SfM is not so optimized as other proprietary software, but is giving good results in terms of cost and availability.

The SfM process allows the computation of the georeferencing errors as the difference between the true location of the GCPs in object space and their estimated position, using SFM, after geometry correction. The values for every site are shown in Table 2 as RMSE values, the global RMSE being 0.09 for x, 0.16 for y, and 0.1 for z. These values are just an estimate of the accuracy, and checkpoints should be used for a sounding estimate.

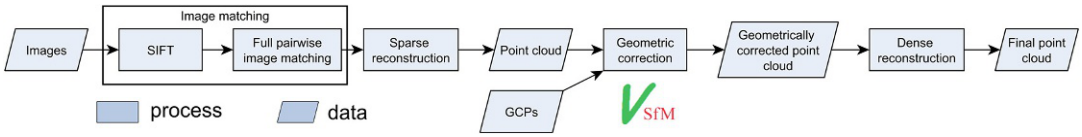

FIG. 3 SfM workflow.

TABLE 2 The RMSE of GCPs after the SfM modeling for every study area.

ID	Name	No. of GCPs	x RMSE	y RMSE	z RMSE
1	Săveni downstream	10	0.061	0.085	0.331
2	Săveni upstream	10	0.174	0.321	0.038
3	Şoldăneşti downstream	8	0.084	0.136	0.008
4	Şoldăneşti upstream	7	0.056	0.085	0.012

3.3.2 *Point cloud postprocessing*

The point clouds obtained through the SfM approach are much denser than the LiDAR points (Table 3) but can be processed in a similar manner. The MCC filtering is much more aggressive because not as many points cross to the vegetation canopy. Even in cases with low vegetation cover, such as ours, the results of the MCC filtering are not always good enough and manual editing is needed (Fig. 4). Another type of error typical of SfM point clouds is the presence of points with low altitude (several meters under the point cloud), which were identified and deleted using the height above ground point (relative elevation) in CloudCompare (https://www.danielgm.net/cc/).

3.4 DEM generation

The quality of DEMs is highly influenced by the interpolation method, and by the density of the input data (Heritage et al., 2009). Regarding this, the density of data in the case of LiDAR and UAV photogrammetry is enough in order to depict morphologies that have decimeter extents. The choice of interpolator is secondary to the data density, but in general TIN interpolators have the lowest errors (since every point is honored) and can represent linear features (Heritage et al., 2009). Kriging was used with success (Lloyd and Atkinson, 2002) and is more statistical sounding, but it can give noise. Although we agree with this statements, TIN algorithms create hard edges that are not seen in nature, especially in areas where the data density is lower, so we used a spline interpolator that has characteristics that are able

TABLE 3 The details of SfM point cloud data.

ID	Name	Flight date	Density (points/m^2)	Mean spacing (m)	Density of ground points (points/m^2)	Mean spacing of ground points (m)
1	Săveni downstream	02/17/2019	32.36	0.0000013	31.98	0.0000013
2	Săveni upstream	02/17/2019	32.11	0.0000013	31.73	0.0000013
3	Şoldăneşti downstream	03/24/2019	77.12	0.0000009	76.93	0.0000009
4	Şoldăneşti upstream	03/24/2019	54.48	0.0000008	52.43	0.0000008

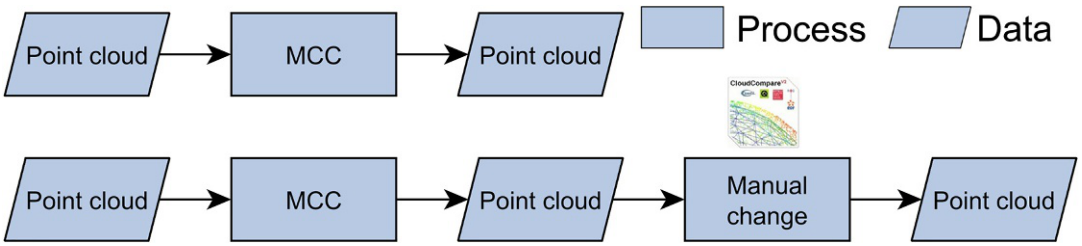

FIG. 4 Postprocessing workflow of point clouds.

to allow the surface to pass through the input points (so it honors them as in TIN) and to minimize spatially the bending of the surface, especially in case of densely spaced data (Niculiţă, 2012). Of course, some overshooting is to be expected, but it should be restricted to areas where the density of elevation data is sparse.

DEMs were interpolated from the LiDAR and SfM point clouds with a multilevel B-spline (MBS) (Lee et al., 1997) at a resolution of 0.25 m. The chosen resolution was reflecting a compromise between data density, data coverage, image resolution, efficient data storage/later processing requirements, and surface representation. According to Hengl's (2006) specification, the point density is showing an optimum pixel size between 0.13 and 0.23 m, whereas the lowest mean distance between neighbor points is 0.26 m. The 0.25 m value was considered a good trade-off.

MBS is an algorithm that well controls the spline interpolation, through the use of successive quadtree levels and generates relatively smooth data compared to a TIN interpolator (Niculiţă, 2012), which will generate hard edges and planar surfaces, especially since the data density is good (the maximum distance between neighbor points is between 0.8 and 1.8 m). The MBS settings that control the degree of generalization of data are the maximum level of interpolation and the threshold of error allowed. Maximum level 14 allows for every point to influence the model, and we have chosen this value. A threshold error of 0.01 will smooth the surface more than a 0.001 error threshold. In Fig. 5, several runs of these settings with variable values to show their influence are represented (the highlighted run represents the chosen parameter values).

For the studied sites, the mean vertical accuracy of the LIDAR DEM versus the GCPs used for SfM georeferencing is 0.1 m. The mean vertical accuracy (expressed as the RMSE of elevation difference) of the SfM DEMs computed for the 35 GCPs is 0.15 m (Table 4).

3.5 Geomorphic change detection

Geomorphic change detection (GCD), a type of DEM differencing (Brasington and Smart, 2003) or DEM of differences (Wheaton, 2008), was applied in our study. For the GCD analysis,

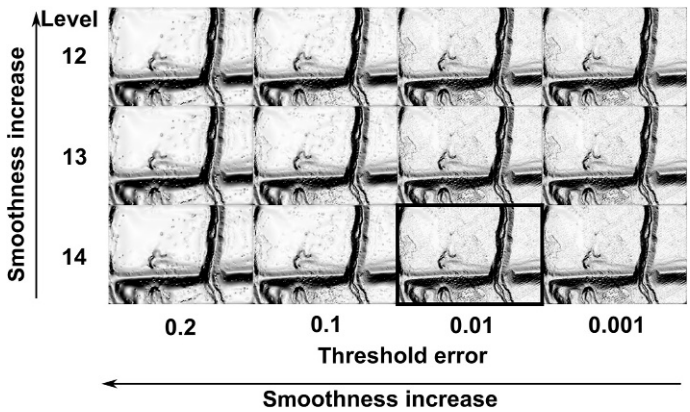

FIG. 5 MBS interpolation settings and their results.

TABLE 4 The RMSE of the DEMs for every study area.

ID	Name	No. of GCPs	LiDAR DEM z RMSE [m]	SfM DEM z RMSE [m]
1	Săveni downstream	10	0.363	0.405
2	Săveni upstream	10	0.004	0.039
3	Şoldăneşti downstream	8	0.005	0.053
4	Şoldăneşti upstream	7	0.026	0.116

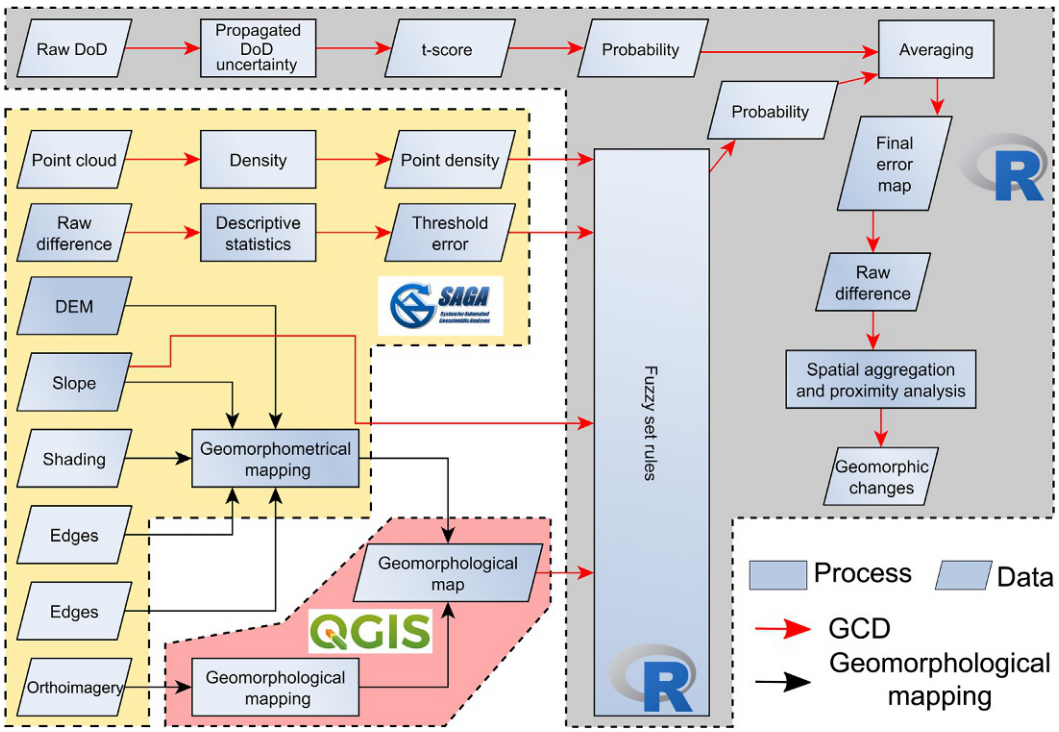

FIG. 6 The GCD workflow.

we have used the approach of Wheaton (2008), later extended in Wheaton et al. (2010) and Bangen et al. (2016). Instead of using the software provided by Riverscapes Consortium (http://gcd.riverscapes.xyz/), we have implemented the methodology in R stat (R Core Team, 2013) using various packages and SAGA (Conrad et al., 2015) software (Fig. 6).

The Wheaton mixed approach (Wheaton et al., 2010) can be divided into four main steps: (i) the computation of raw differences between a reference and a later DEM; (ii) the error modeling; (iii) the error filtering; and (iv) the construction of the sediment budget. The first step is straightforward and was implemented as a raster algebra difference. In the second step, two uncertainty thresholding approaches were used: the 95% confidence interval of spatially uniform standard deviation of raw differences (0.0355 m for Săveni downstream, 0.0212 m for Săveni upstream, 0.0193 m for Șoldănești downstream, and 0.0167 m for Șoldănești upstream), and the probability of spatially variable error using fuzzy inference rules, in order to incorporate for nonuniform spatial errors. The second was based on a geomorphological mapping of the gully system in 2019, performed on the UAV SfM high-resolution DEM, its derivatives (slope, edge detection of slope, compound shading), and the orthoimage; a threshold of error was assigned for every digitized polygon in QGIS. The error was computed from the relatively flat areas of the reservoir bottom from around every polygon using descriptive statistics, areas that are stable from a geomorphological point of view. The values of the error were between ±0.1 and ±0.5 m, estimated based on the interquartile range. Further, the threshold error was filtered by probabilities that were assigned based on the point density of the LiDAR and UAV SfM data, slope (as in Wheaton et al., 2010), and vegetation cover assessment using fuzzy set rules (instead of the 3D point quality of Wheaton et al., 2010). The fuzzy set rules were created with R stat package FuzzyR (Garibaldi et al., 2017). For point density and slope, trapezoidal membership function was used with the left foot, left shoulder, right shoulder, right foot values defined based on the descriptive statistics of the input data (Fig. 7 and Table 5), whereas for vegetation the

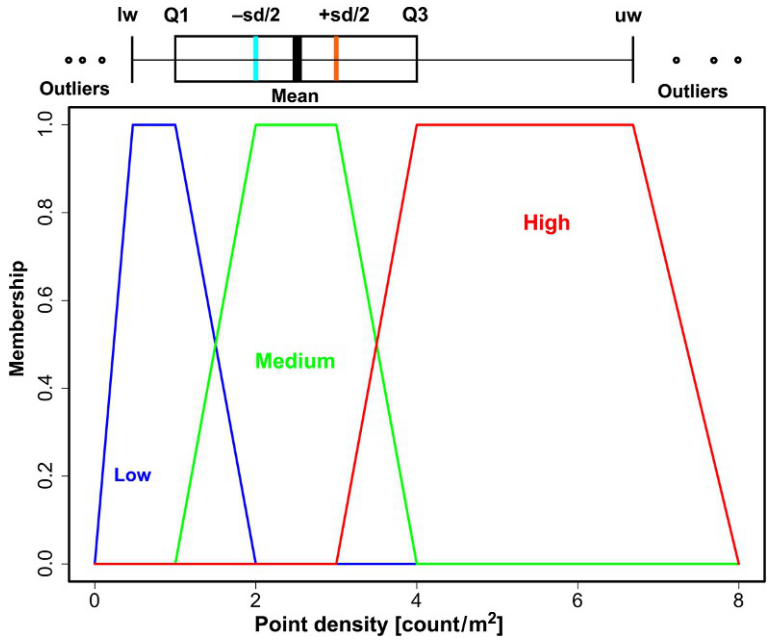

FIG. 7 The fuzzy set membership computed based on descriptive statistics of data thresholds.

TABLE 5 The values of the trapezoidal membership function.

ID	Name	Year	Variable	min	lw	Q1	Mean	sd	Q3	uw	max
1	Săveni downstream	2012	PD	0.00	0.00	1.00	1.98	1.14	3.00	6.00	8.00
			SL	0.00	0.00	2.56	8.98	9.02	12.55	27.54	63.39
		2019	PD	0.00	22	29	31.84	5.09	34	41	70
			SL	0.00	0.00	2.36	8.57	8.78	11.71	25.74	86.46
2	Săveni upstream	2012	PD	0.00	1.00	2.32	1.99	2.67	3.48	5.22	57.38
			SL	0.00	0.00	0.00	5.72	8.46	8.02	20.07	74.32
		2019	PD	0.00	0.00	0.00	18.24	16.28	32.26	63.81	63.81
			SL	0.00	0.00	0.00	4.96	7.97	6.43	16.08	72.56
3	Şoldăneşti downstream	2012	PD	0.00	0.00	0.00	0.83	0.97	2.00	5.00	5.00
			SL	0.00	0.00	0.00	3.58	6.74	4.23	10.58	67.11
		2019	PS	0.00	0.00	0.00	25.59	27.18	53.00	120	120
			SL	0.00	0.00	0.00	3.93	7.17	4.85	12.12	73.89
4	Şoldăneşti upstream	2012	PD	0.00	1.00	1.00	1.16	0.58	1.00	1.00	4.00
			SL	0.00	0.00	1.38	6.83	7.26	9.46	21.59	62.17
		2019	PD	0.00	61	73	78.03	8.49	81	93	169
			SL	0.00	0.00	2.49	7.69	7.57	10.14	21.61	80.68

lw, lower whisker; *PD*, point density, *SL*, slope; *uw*, upper whisker.

singleton membership function was used. When the minimum, the lower whisker, and Q1 were equal, Q1 was computed as half of the mean. This statistical setting of computing the trapezoidal function membership was chosen in order to standardize the fuzzy membership assignation.

The fuzzy inference system was of type Mamdani with minimum for AND and maximum for OR methods. The fuzzy rules are identical with those of Wheaton et al. (2010). The convolution filter for deriving the spatial contiguity index for erosion and deposition coherence was applied with the *focal* function of the *raster* R stat package (Hijmans, 2017) for the joined probabilities (uniform and spatially variable).

In the final stage, the sediment budget was computed for every type of process, using again the geomorphological map. Error assessment was performed only based on the uniform spatial filter, and as the overall figure for erosion and deposition (Table 6).

3.6 Geomorphological mapping

Geomorphological mapping was performed through a geomorphometric approach on the SfM DEM using orthoimagery as a visual aid. Slope, edge detection of slope, and compound

TABLE 6 The areal and volumetric GCD data for each gully.

		Săveni downstream	Săveni upstream	Șoldănești downstream	Șoldănești upstream
Area [m^2]	2012	6259	16,237	9091	8534
	2019	8340	19,190	9806	9284
Area change [m^2] (%)		2081 (33%)	2953 (18%)	715 (8%)	750 (9%)
Erosion area [m^2]	Raw	5077	7219	3929	1370
	Thres.	2491	1190	883	854
Deposition area [m^2]	Raw	3263	11,971	5877	7914
	Thres.	783	2308	979	4628
No change area [m^2] (%)	Raw	—	—	—	—
	Thres.	5066 (61%)	15,692 (82%)	7944 (81%)	3802 (41%)
Eroded volume [m^3] (%)	Raw	2474 ± 180	1598 ± 153	699 ± 76	663 ± 23
	Thres.	1847 ± 88	622 ± 25	334 ± 17	548 ± 14
Deposited volume [m^3] (%)	Raw	844 ± 111	2909 ± 243	851 ± 109	652 ± 127
	Thres.	375 ± 28	707 ± 47	100 ± 18	410 ± 74
Net volume [m^3] (%)	Raw	1631 ± 69	-1311 ± 91	-152 ± 33	11
	Thres.	1472 ± 61	-85 ± 22	234 ± 1	138 ± 60

shading were the DEM derivatives used to identify the breaks in the morphology that correspond with the visual information from the orthophoto map interpretation. Digitization was performed in QGIS v 3.6 by creating polygons that correspond to elements of the gully, by checking in 3D view the results, and refining if needed. Besides the 2019 data, aerial imagery from 2003 and 2010 at 0.5 m resolution, and Google Earth time lapse imagery were used to check for the state of the geomorphological processes as well. These data were used to qualitatively assess the state of the bank erosion, channel deposition, landslide areas, vegetation cover, and reservoir bottom lateral to the gully. According to the literature on gully morphology (Ireland et al., 1939; Heede, 1976; Imeson and Kwaad, 1980; Bettis and Thompson, 1985; Geyik, 1986; Bocco, 1991; Farres et al., 1993; Poesen et al., 1996, 1998), the following elements of a continuous gully were delineated (Fig. 8): edge, ridge, bank, terrace, bottom, channel, and alluvial fan. The bank, the channel, and the bottom were split into parts at the main branches of the main gully, at the knickpoints, at the headcuts, and for bank gullies. Bank landslides (slumps) triggered by sloughing and incision were also separated. Piping was not identified as an important process along the investigated gully systems, although there are important systems of cracks in the silty sediments of the reservoirs through which water is moving. From this point of view, most probably the hydrogeological factors involved in gully evolution are the presence of a groundwater body inside the reservoir sediments bounded by the old alluvial bed, and sediment depth which also controls the depth of the gully

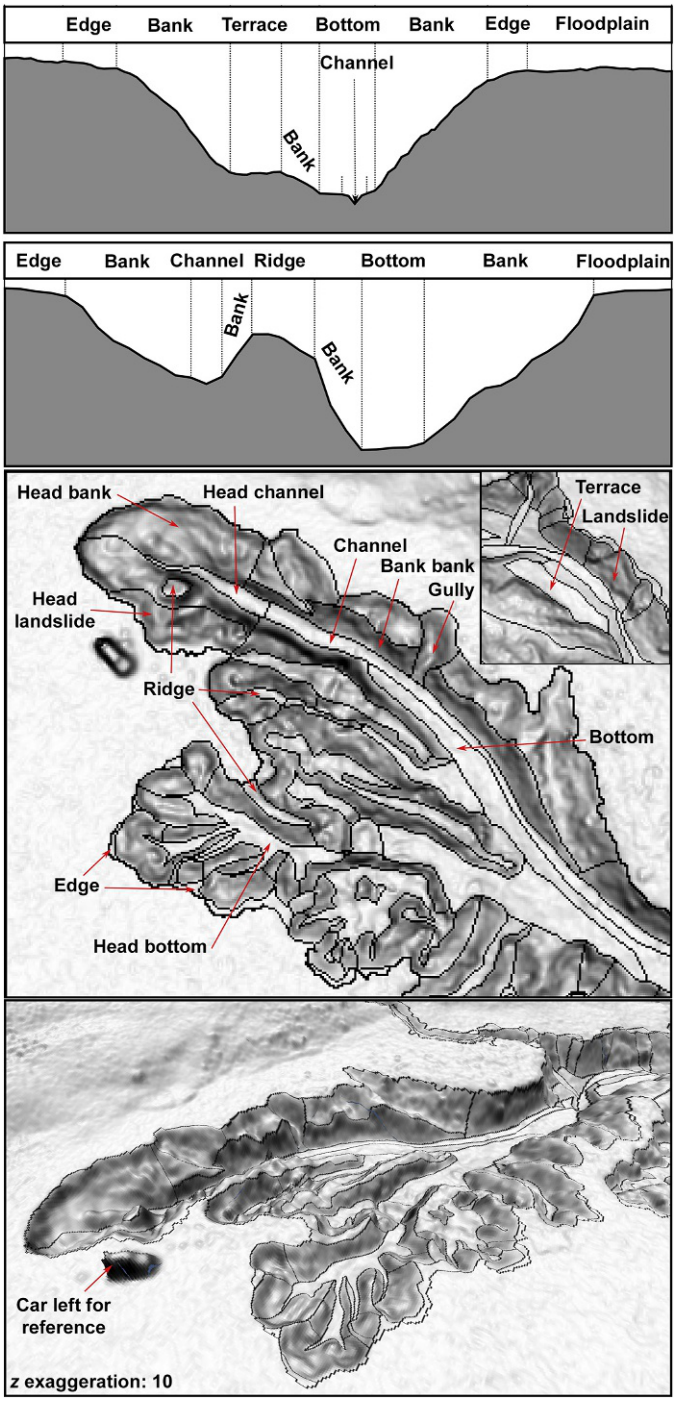

FIG. 8 The geomorphological mapping of the gully elements shown on topographic sections (*top*), on 2D (*middle*), and 3D shading (*bottom*).

(Mărgărint et al., 2017a,b; Niculiţă et al., 2017). These reservoir bottom gullies evolve from a small channel incision upstream from the dam breach, by deepening from the initial reservoir bottom, and head migration upstream where there is an overland flow concentrating in the dam breach area. As the gully extends upstream, channel incision, slope wash, and landslides generate the bank retreat and the gully will widen at the same time as it gets deep. The episodes of incision happening along the gully generate the presence of knickpoints and of sediments along the channel and the bottom, and even of terraces. This situation is somehow similar to hillslope or valley gullies (Bocco, 1991), with the difference that the discontinuity of the process is not present. Instead, when the discharge is not present and vegetation grows on the banks and the bottom, the gully will stabilize. Later, when overland flow appears, the gully might reactivate, especially in the head areas. The discontinuity is only present in the gully-channel system, some gullies continuing downstream with channels (Săveni gullies), others not (Şoldăneşti gullies), and the presence of gully fans is mainly characteristic for the ones that do not continue with a channel downstream (as is the case for Şoldăneşti upstream). These reservoir bottom gullies (Niculiţă et al., 2017) have various forms (Imeson and Kwaad, 1980): linear, bulbous, dendritic, or compound and are of type one or four.

4 Results

The results of the change detection between the 2012 LiDAR DEM and the 2019 UAV SfM DEM are represented in multiple ways. In Figs. 9–12 for every investigated gully, the 2012 LiDAR DEM shading and the raw differences are represented side by side. Besides the gully border, the ground control points and the location of the topographic sections are displayed.

The values from Table 6 show the areal extension of the gully systems from 2012 to 2019, split by erosion, deposition and no change, and the volumetric data with errors for the raw and the thresholded data. The Săveni downstream gully has the biggest expansion, both in terms of surface and volumes of sediments, followed by Săveni upstream. Şoldăneşti downstream and upstream gullies have the lowest activity. The errors vary between 4% and 25% of the volumes.

In Figs. 13, 16, 19, and 22, the filtered GCD final results are shown on the 2019 UAV SfM DEM shading, with the gully border, topographic sections (shown in Figs. 14, 17, 20, and 23), and field photography (shown in Figs. 15, 18, 21, and 24) locations. The histograms of the GCD raw and filtered results are shown in Fig. 25, whereas the geomorphological mapping (Fig. 26) was used to separate the volumes for every gully element (Fig. 27).

The Săveni upstream gully (Fig. 15, P2) is showing important erosion by head retreat at the one branch along the main section (the one toward the northwest), and at two branches that develop along the Iazul Mare valley, to the northeast (Fig. 13, P1, Fig. 14, sections 2 and 4, and Fig. 15, P3, P4, and P10). The banks outside the heads do not show important erosion processes (Figs. 13 and 14, section 3, Fig. 15, P5–P10, and Fig. 27), but patches of basal accumulation due to erosion and landsliding at the upper part of the profile (Fig. 15, P3), and due to their length accumulate a greater amount of deposition than erosion (Fig. 27). The gully bottom and channels have the most important areas of deposition (Figs. 13 and 14, sections 1 and 4, Fig. 15, P5–P9, and Fig. 27), downstream the gully heads and knickpoints (Fig. 15, P3 and Fig. 27). The incised channels, terraces, and bottom from 2012 were covered by sediments

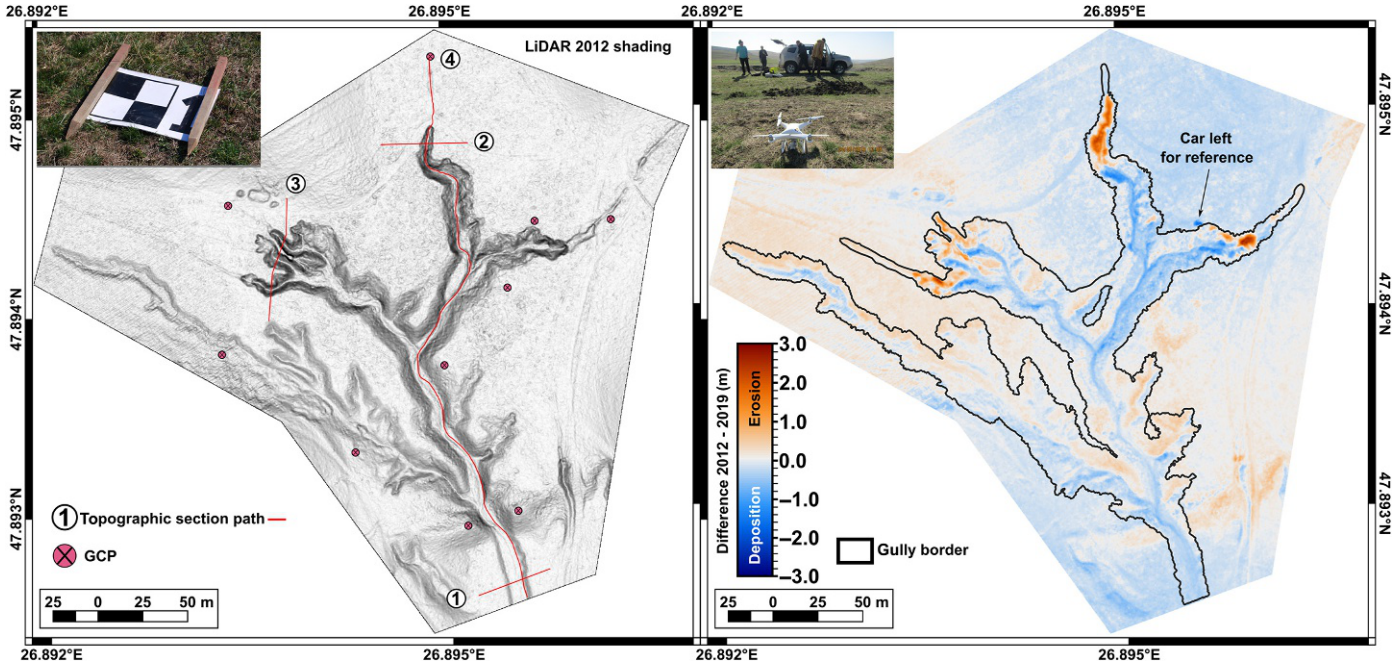

FIG. 9 Săveni upstream, GCP location, topographic sections location, and GCD raw raster: 1–4 are the paths of the topographic cross-sections from Fig. 14.

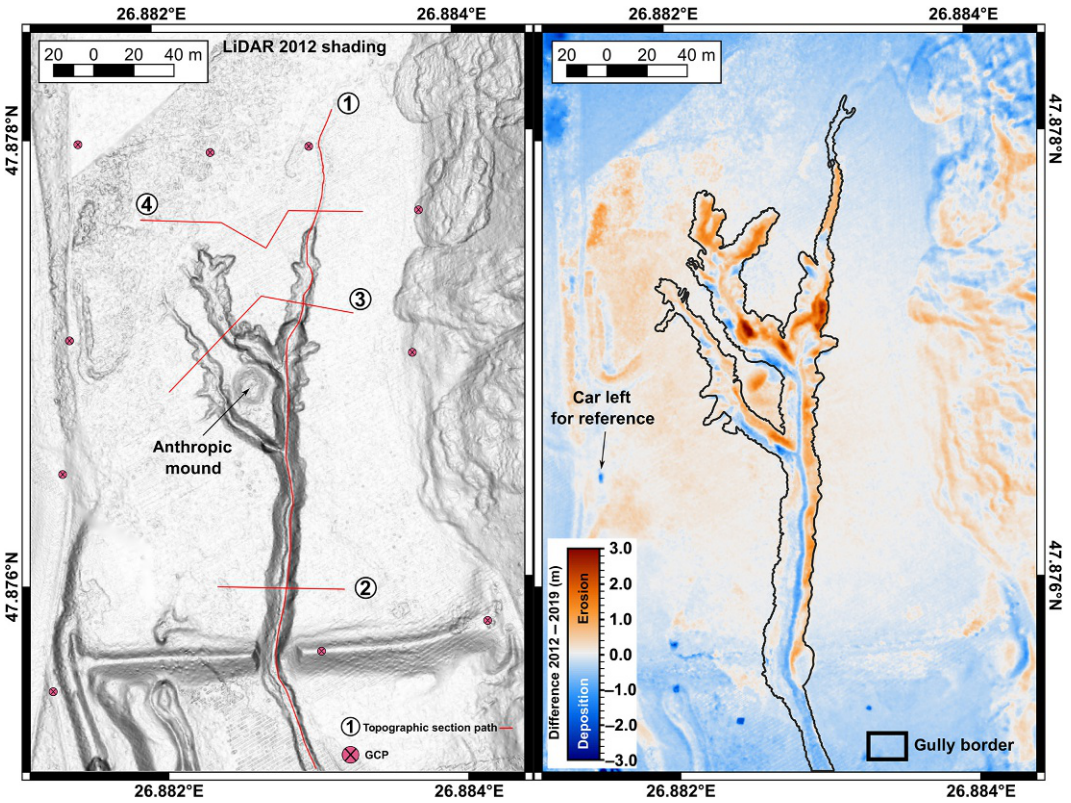

FIG. 10 Săveni downstream, GCP location, topographic sections location, and GCD raw raster: 1–4 are the paths of the topographic cross-sections from Fig. 17.

until 2019 (Fig. 14, sections 1 and 4, and Fig. 15, P5–P9). The first branch that develops toward the northwest along the main valley at the contact with the hillslope (Figs. 13 and 15, P2) is inactive, affected by landslides at the hillslope side and by anthropic intervention (Fig. 26), the head being transformed into a small reservoir by damming (Fig. 13). The erosion and deposition are balanced (Fig. 25), both over 600 m^2, with deposition slightly bigger (net deposition of approx. −85 m^3) (Fig. 25). These results are showing that the gully is unable to evacuate all the sediments produced.

The Săveni downstream gully (Fig. 18, P3) is showing important erosion by headward retreat not only at the main head and at two secondary heads (Figs. 16 and 17, sections 1, 3, and 4, and Fig. 18, P1, P2, P4, and P8), but also at two knickpoints on the main branch and on a secondary one (Figs. 16 and 17, sections 1 and 4, and Fig. 18, P2, P4, and P6–P7). The left bank of the main branch is also eroded along the section downstream of the knickpoint (Figs. 16 and 17, section 2, and Fig. 18, P7 and P9), whereas the channels are usually filled with sediments by deposition (Figs. 16 and 17, sections 1 and 2, and Fig. 18, P2, P4, and P7–P9). The erosion is predominant (Fig. 25) and characterizes the banks and the bottom with important landslides (Fig. 18, P9 and Fig. 27), but is more important on banks outside the heads. Deposition characterizes the main channel and bottom with up to 1 m of sediments (Fig. 17, sections 1 and 2).

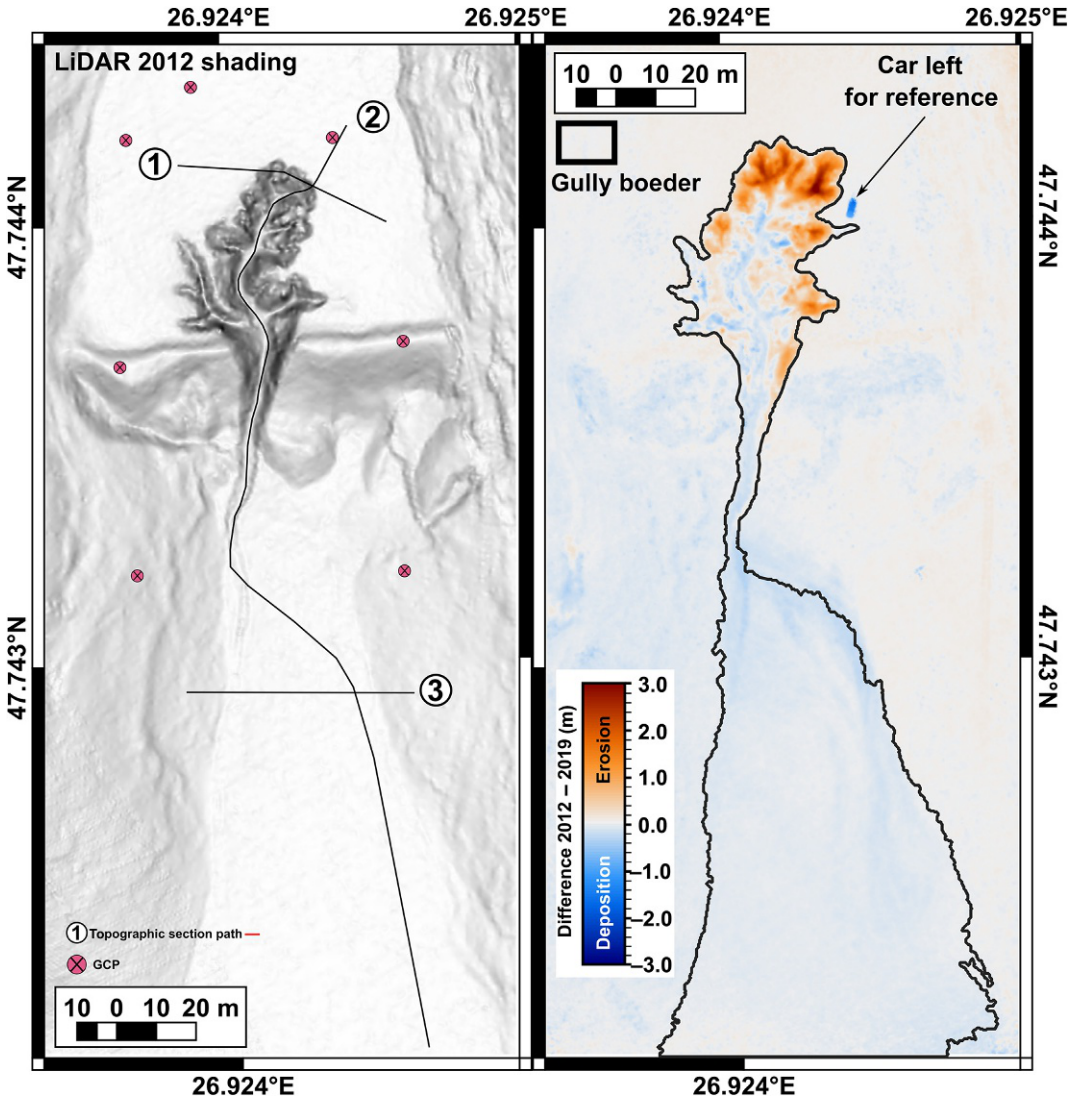

FIG. 11 Şoldăneşti upstream, GCP location, topographic sections location, and GCD raw raster: 1–3 are the paths of the topographic cross-sections from Fig. 20.

Human impact also occurs by deposition of the sediments of an anthropic mound (Fig. 10) at the bank of a secondary branch (Figs. 16 and 18, P6). The erosion is almost five times bigger than deposition, with a net erosion almost four times bigger than deposition (Fig. 25). These data are showing that the majority of the eroded sediment has been evacuated from the gully (80%).

The Şoldăneşti upstream gully is showing erosion by head and bank retreat along all the branches (Figs. 19 and 20, sections 1 and 2, Fig. 21, P1–P3, and Fig. 27) and slight deposition along the channels (Figs. 19 and 20, section 2, Fig. 21, P4–P5, and Fig. 27). The most interesting point is that the main deposition is on the alluvial cone (Figs. 19 and 20,

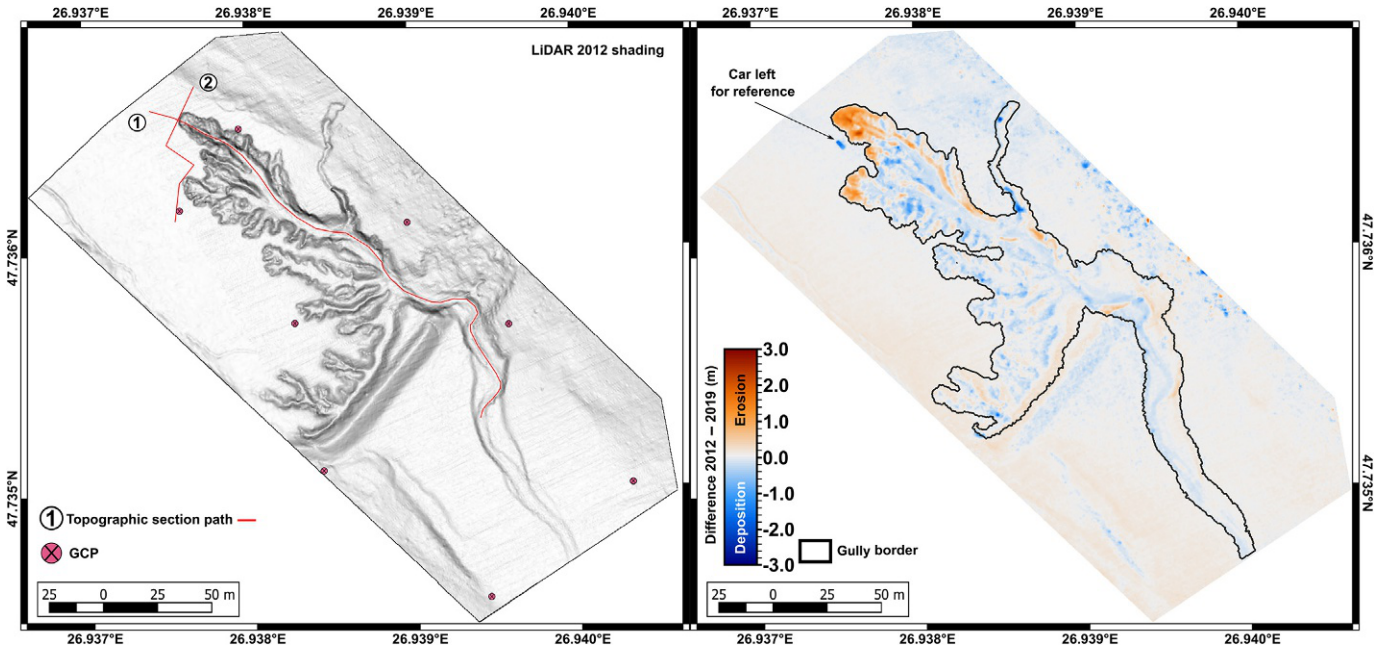

FIG. 12 Şoldăneşti downstream, GCP location, topographic sections location, and GCD raw raster: 1–2 are the paths of the topographic cross-sections from Fig. 24.

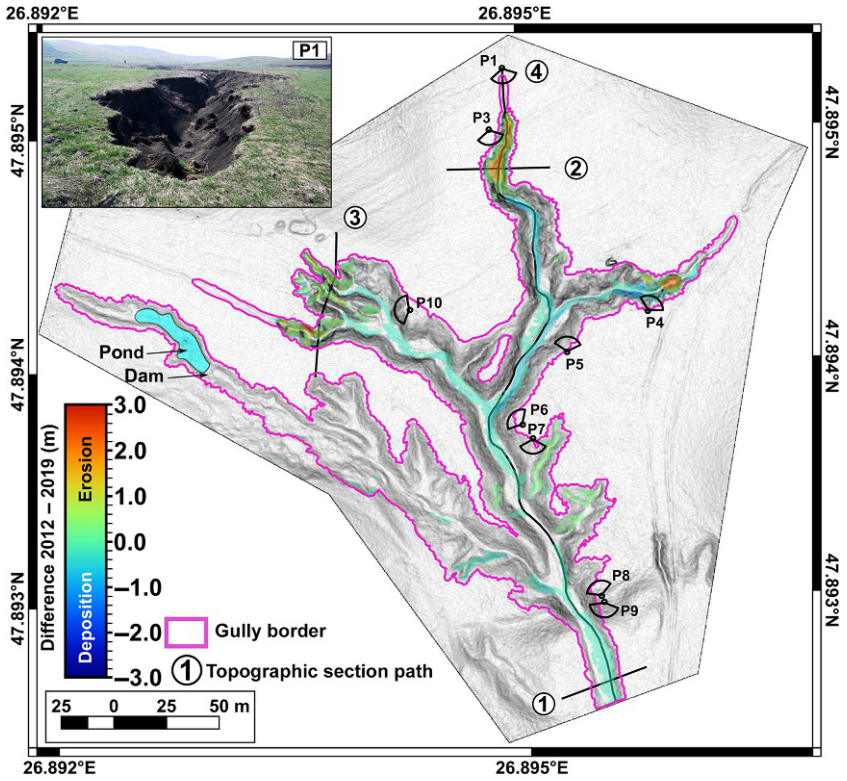

FIG. 13 Săveni upstream change detection results: 1–4 are the paths of the topographic cross-sections from Fig. 14.

section 3, Fig. 21, P4, and Fig. 27). A big proportion of this deposition happened on the gully fan, during a rain event in May 2018, and is visible on the orthophoto image because vegetation did not completely cover the sediments (Fig. 20, section 3, Fig. 21, P4, and Fig. 27). The erosion is slightly bigger than the deposition, with a net erosion of about 139 m^3 (Fig. 25), and both are quite important considering the small size of the gully, which shows important activity. The difference of 25% in eroded sediment volume was evacuated downstream from the gully fan, out of the gully system.

The Şoldăneşti downstream gully is showing erosion mainly by head retreat and head landslides on the main branch and on a secondary one (Figs. 22 and 23, section 2, Figs. 24 and 27). Erosion has also occurred on the main bank (Fig. 27), with slight deposition along the bottoms and channels (Fig. 22, P1 and Fig. 21, section 1), whereas landslides and slope wash generated accumulation at the base of the banks. The erosion is slightly greater than the deposition, with a net erosion of about 234 m^3 (Fig. 25), showing that the 70% of the eroded volume was evacuated from the gully system.

Overall erosion is greater than deposition for all the gullies, except for Săveni upstream, where deposition is slightly predominant (Fig. 25). This is showing us that the gully systems in general are able to evacuate between 25% and 80% of the produced sediments through

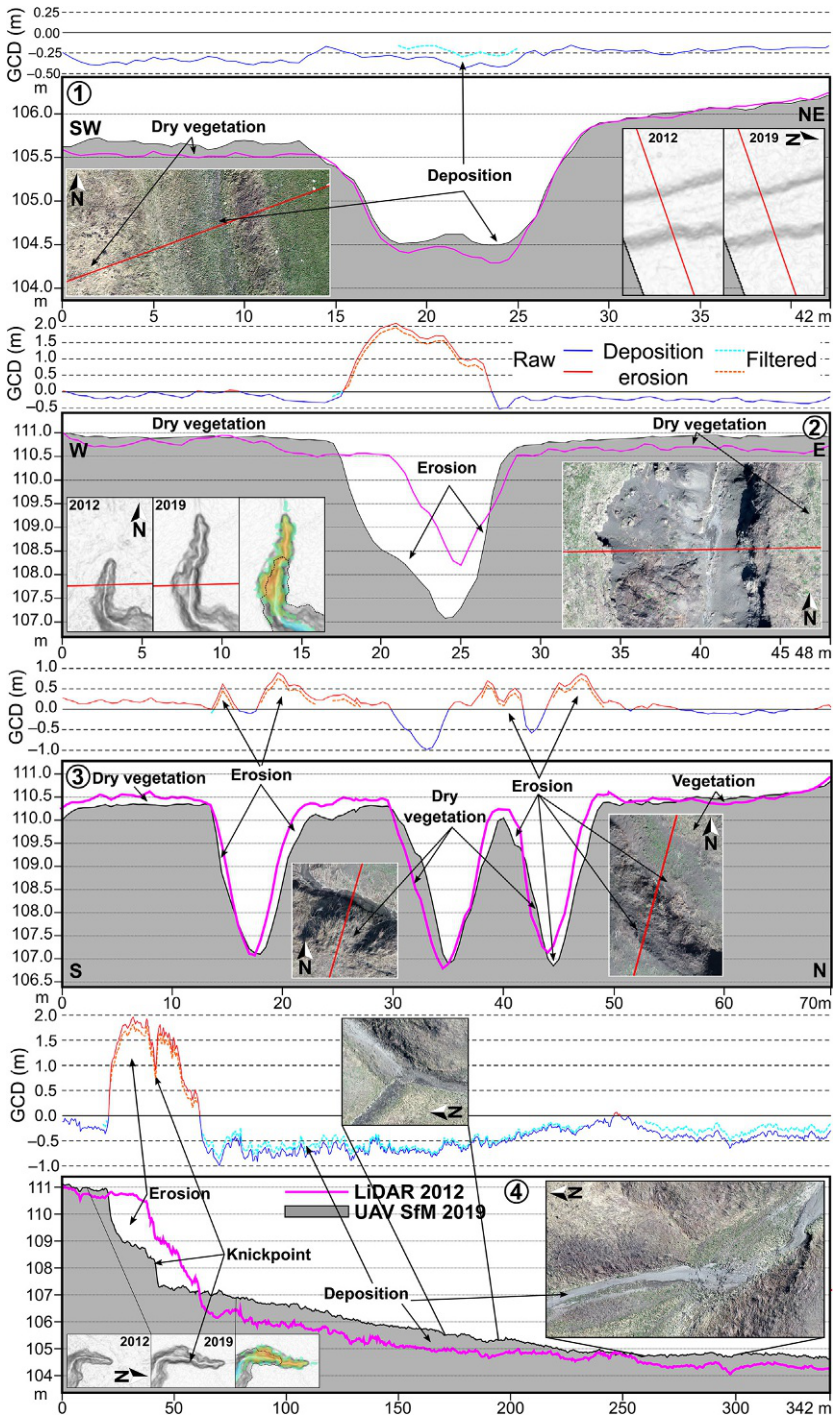

FIG. 14 Săveni upstream topographic and change detection sections (the *red* and *blue lines* represent the raw positive and negative change detection, while the *orange* and the *cyan interrupted lines* represent the final filtered positive and negative change detection results).

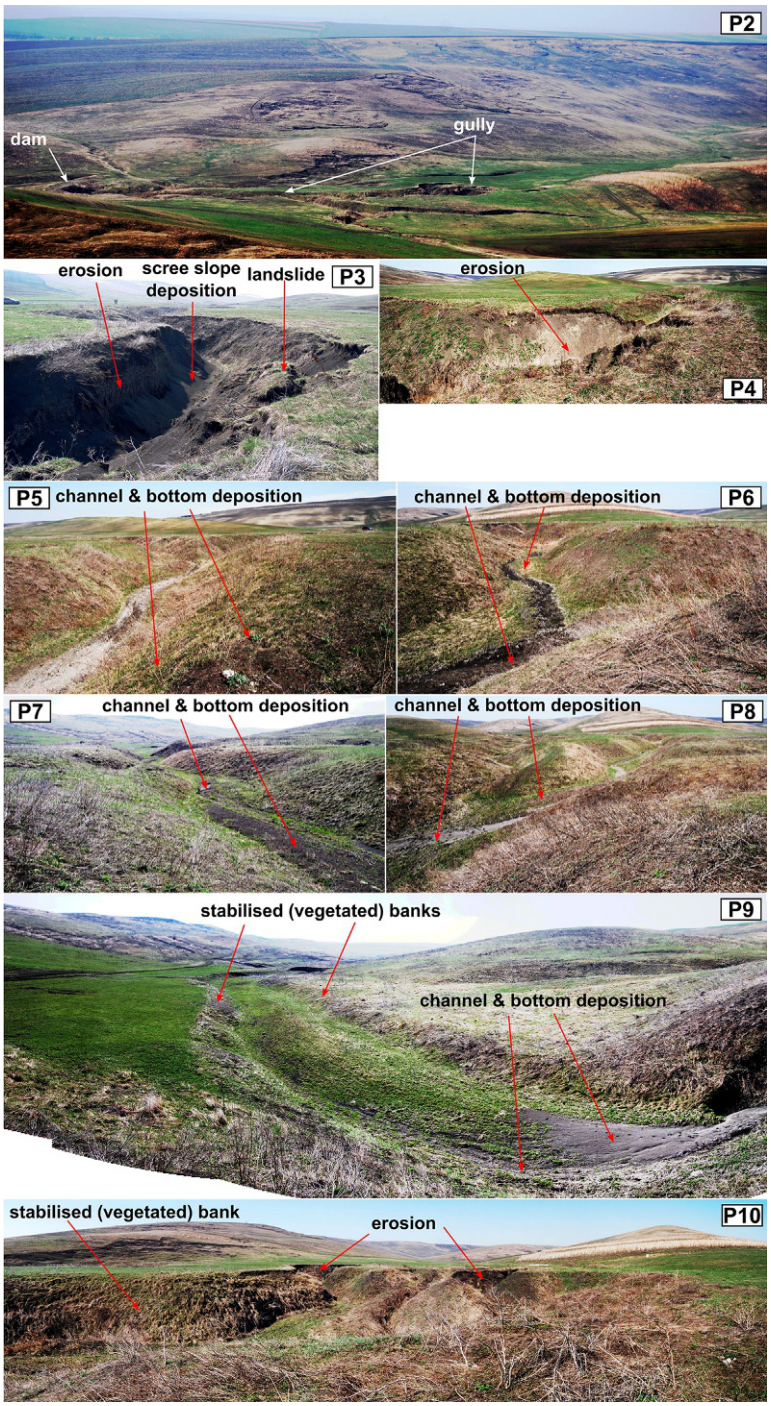

FIG. 15 Săveni upstream field photos (taken 24.03.2019—photo number location is the shown number in Fig. 13).

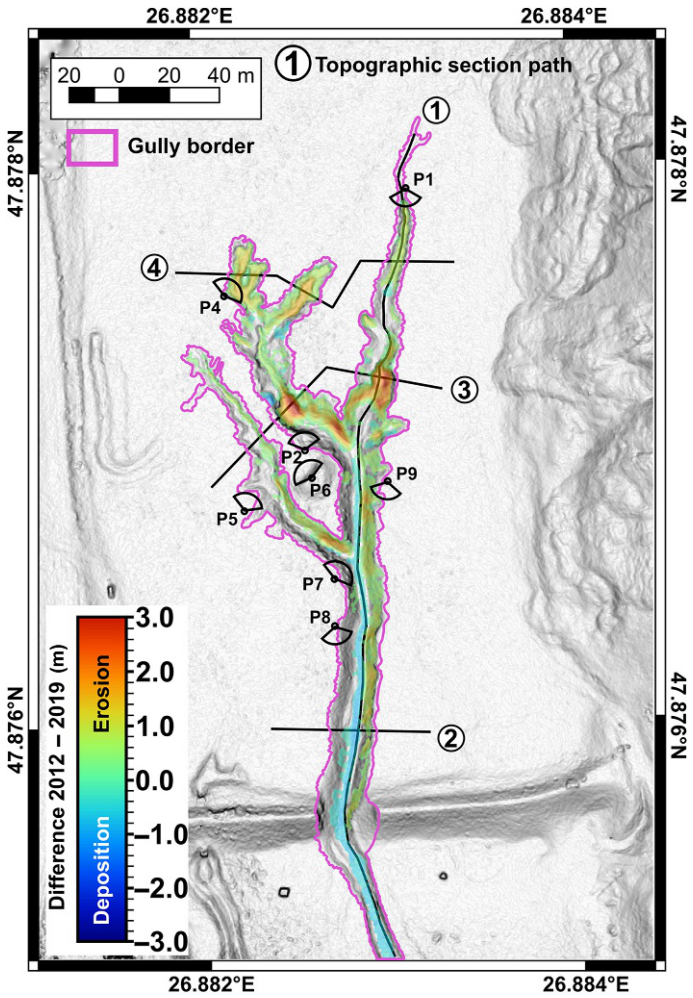

FIG. 16 Săveni downstream change detection results.

erosion. Regarding the gully evolution, the change detection is showing us that the gully heads are the main source of sediment and gully evolution, through erosion of the banks and landslides. The erosion of the banks outside the head areas is in general of secondary importance, except for the Săveni downstream gully, which is the most important in terms of eroded volumes. Deposition appears mostly as channel and bottom aggradation, but important volumes of sediments also were deposited on the banks due to landslides or slope wash. The most active gullies in terms of evacuated sediments are those that have elongated main branches (Săveni downstream and Şoldăneşti downstream). The most active areas of erosion are the nonvegetated ones (Fig. 15, P5–P10, Fig. 18, P4–P9, and Fig. 24), and the most active gullies in terms of both erosion and deposition are Săveni downstream and Şoldăneşti upstream (Figs. 26 and 27).

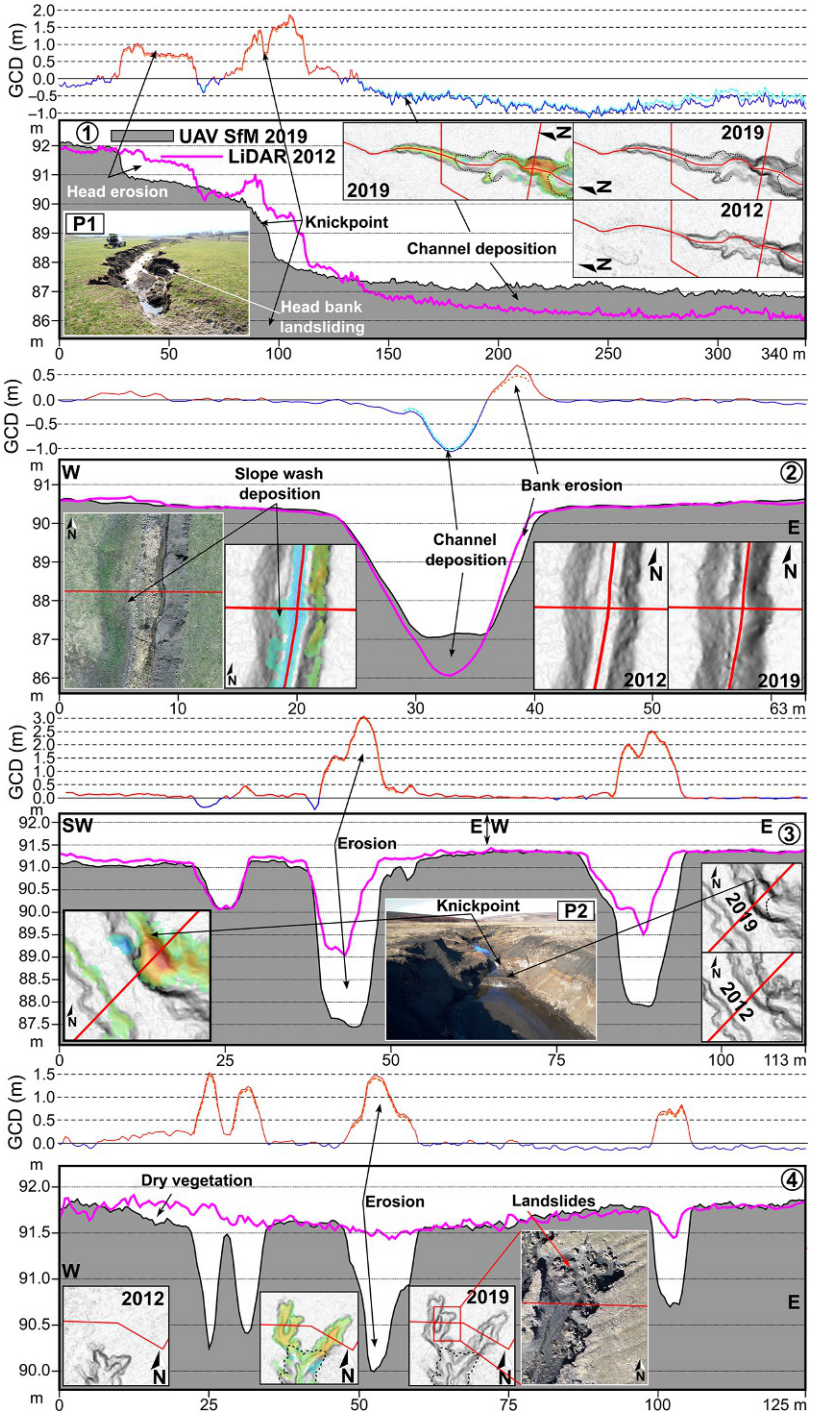

FIG. 17 Săveni downstream topographic and change detection sections.

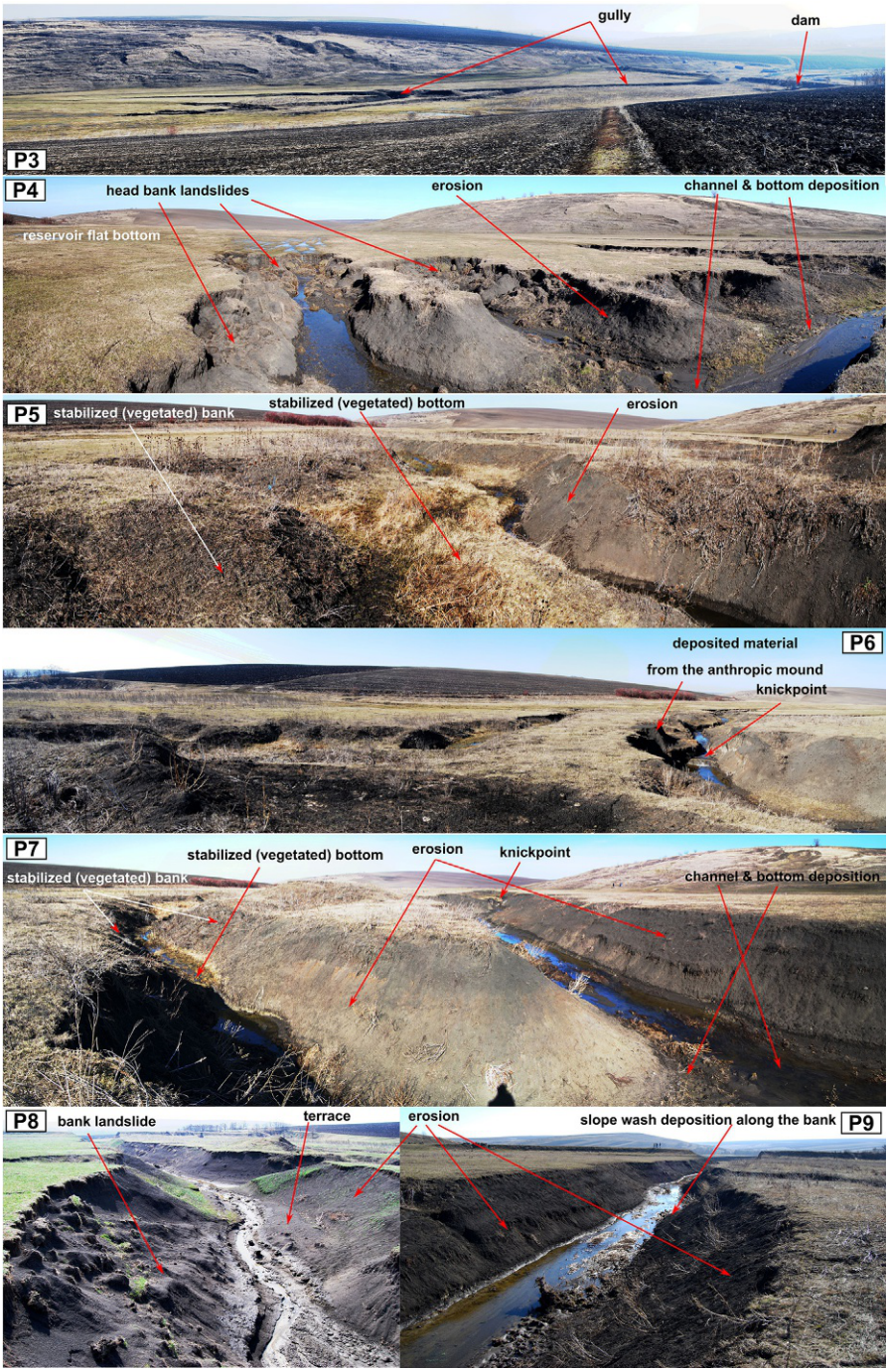

FIG. 18 Săveni downstream field photos (taken 24.03.2019—photo number location is the shown number in Fig. 16).

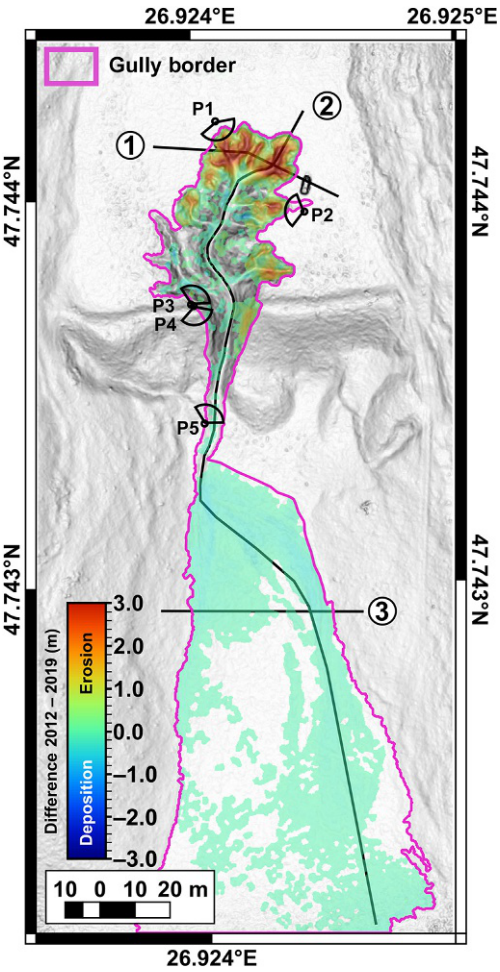

FIG. 19 Şoldăneşti upstream change detection results.

5 Discussions

The comparison between LiDAR and photogrammetry/UAV SfM was performed in the literature qualitatively (Baltsavias, 1999) and quantitatively (Eltner et al., 2013, 2015). Although differences occur in regard to acquisition method and data density, these methods are able to precisely locate the topographic surfaces in the range of several centimeters (Eltner et al., 2015). Further, snow or vegetation can induce positional errors ranging from 10 to 50 cm, as we assessed in our case for the flat areas of the reservoir bottom around the gullies (Fig. 14, sections 1–3, Fig. 17, sections 2–4, Fig. 15, P7–P10, Fig. 18, P5–P9, and Fig. 21, P2). Besides these, the geometry of acquisition can introduce tilts, shifts, and other deformations that are not necessarily linearly correlated. By analyzing the results of the raw differencing between the obtained DEMs (Figs. 9–12), it can be observed that the central area of the study

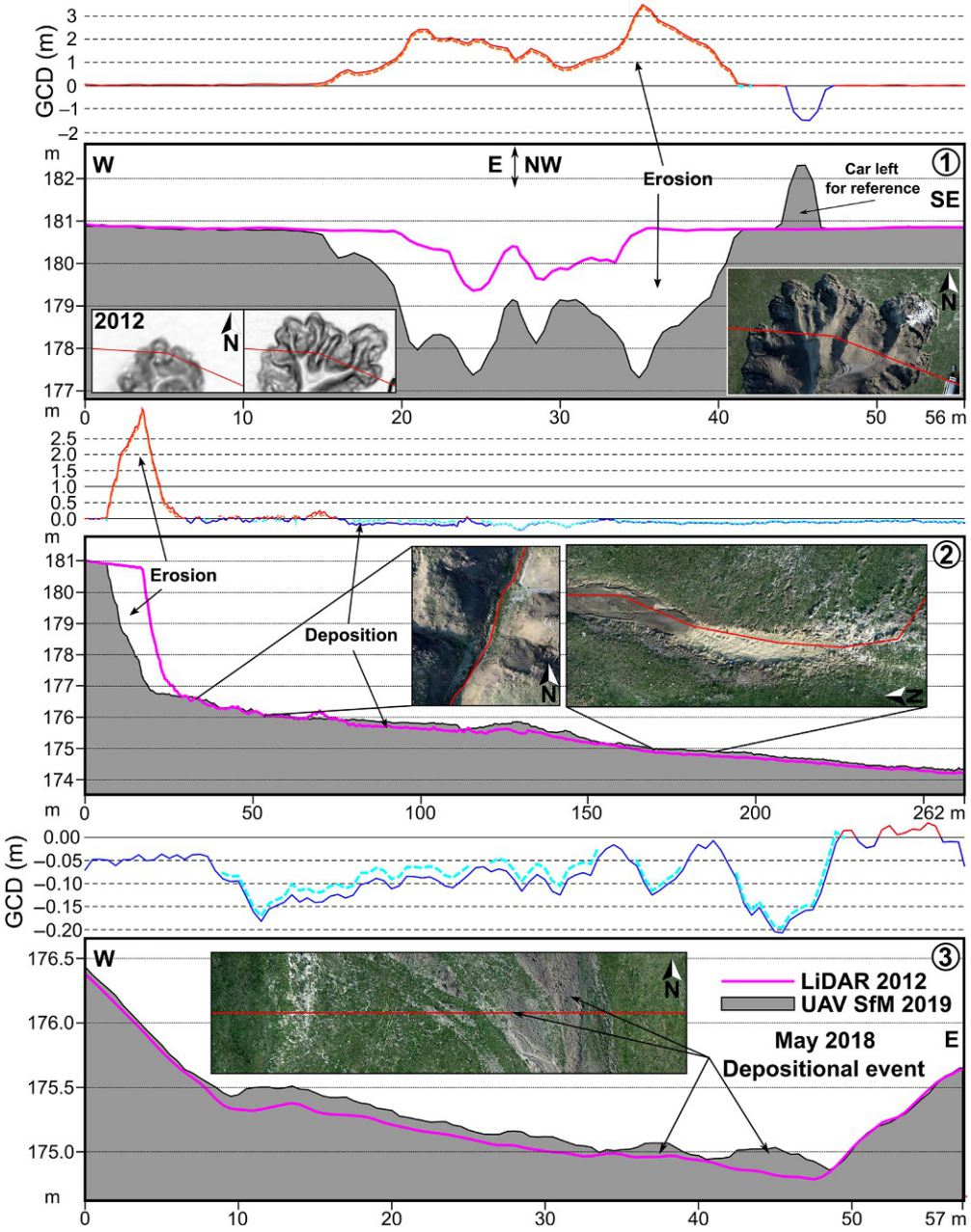

FIG. 20 Şoldăneşti upstream topographic and change detection sections.

FIG. 21 Şoldăneşti upstream field photos (taken 24.03.2019—photo number location is the shown number in Fig.19).

cases has negative values on the floodplain, whereas the edges have positive values or vice versa situations which can be related to the distortion effect of the camera geometry and of the sampling network or to GCP sampling (James and Robson, 2012, 2014). These errors are visible, especially due to the relatively flat area that is surveyed. Because the co-registration differences in elevation are very low in the majority of the studied areas (as can be seen in the topographic section from Figs. 14, 17, 20, and 23), we did not perform co-registration of the point clouds as is done in some cases (Cucchiaro et al., 2018). The main differences between the point clouds are due to geomorphological processes and errors related to snow, vegetation, and SfM deformation.

The LiDAR horizontal accuracy is mainly affected by positioning errors of the carrying platform, of the acquisition system, of the GPS base station data used for georeferencing,

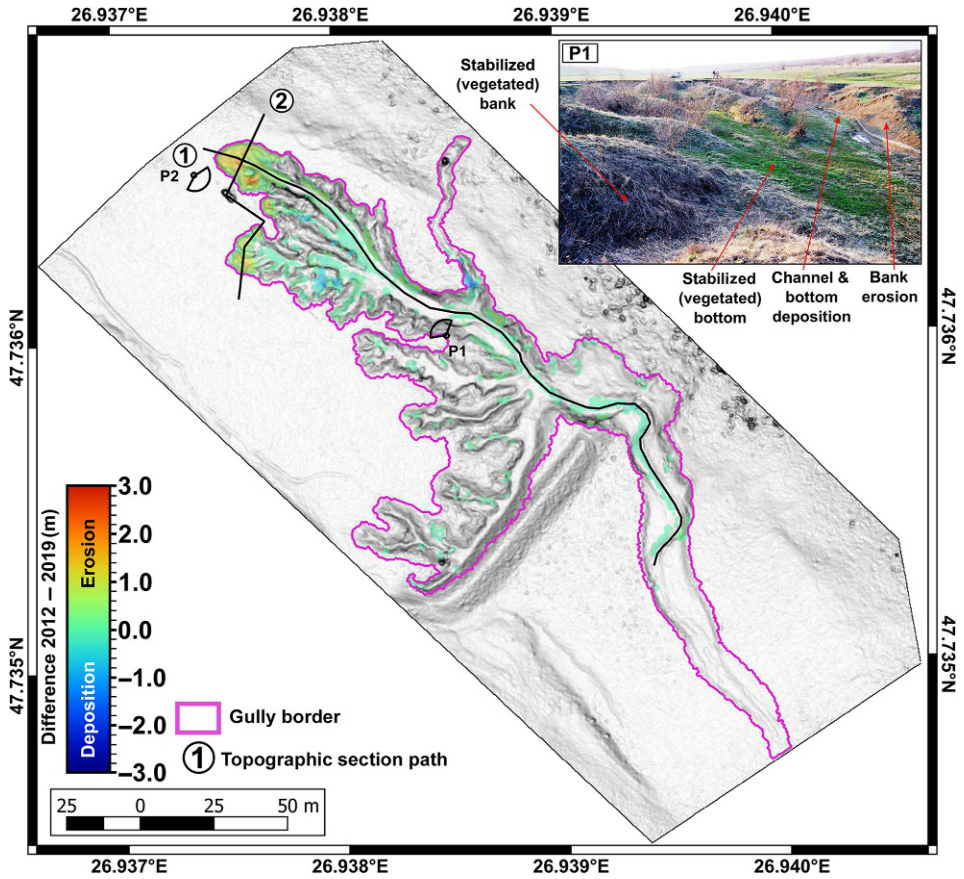

FIG. 22 Şoldăneşti downstream change detection results.

or of preprocessing (ASPRS, 2005), and it is several times greater than the vertical accuracy. The errors associated with the LiDAR data are split into four main groups: error per block, error per strip, error per GPS observation, and error per point (ASPRS, 2004, 2005, 2018). Besides the errors induced by the external factors, which are linear and can be dealt with by operations to the whole dataset, the errors induced by the operations of the platform and of the acquisition system are the most problematic, because they will induce a variable level of error. The boresight error (misalignment between the laser sensor and the navigational and positional system) is variable to flight height, direction, and scan angle, and can be observed in areas with flat gradients, because this affects the scan lines differently. In our case in Figs. 9–12, on the shaded DEM from 2012, these errors can be seen in several areas (for example, in Fig. 9 in the Western part of the DEM, stripes with southwest to northeast orientation can be seen). As can be seen in Fig. 1, for the channel downstream of the dam, these errors can be filtered, but sometimes these will also remove topography, which is why it is preferable that they be dealt with through the change-detection approach. The difference between the striped ground and nonstriped ground is in the range of ± 0.15 m.

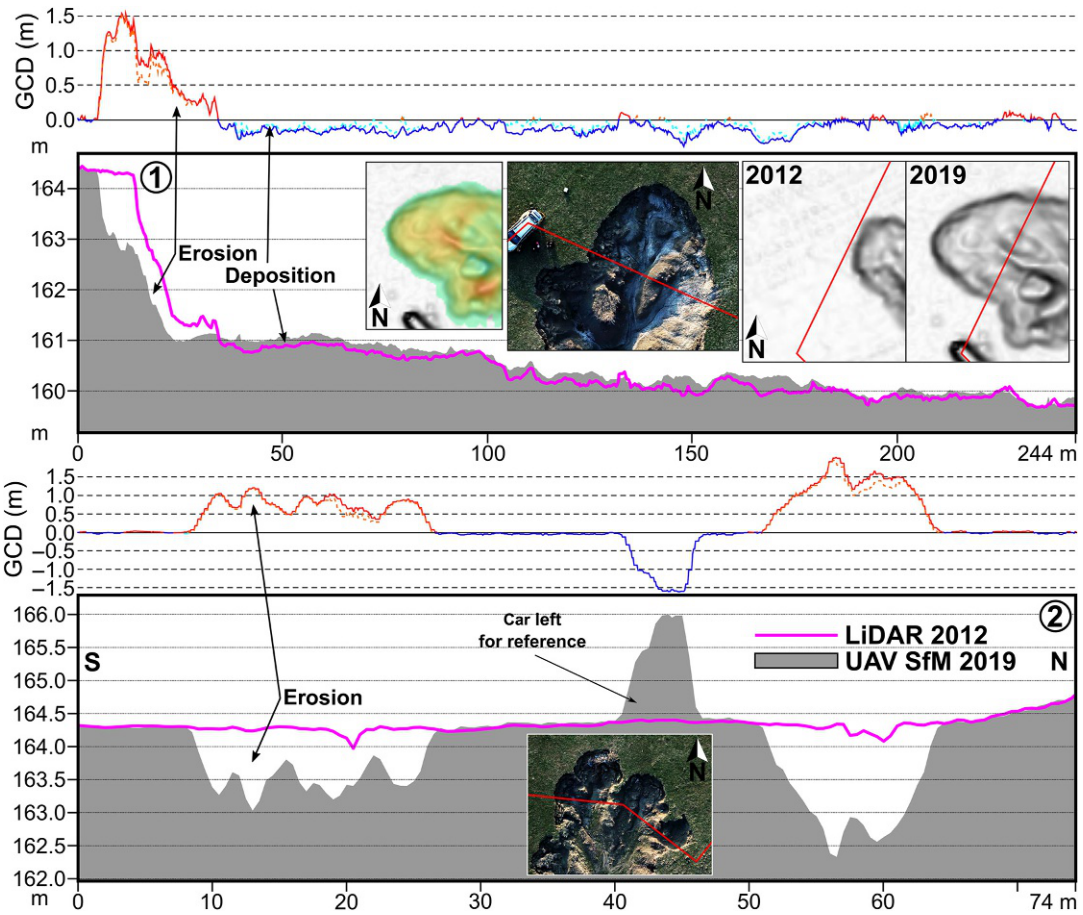

FIG. 23 Şoldăneşti downstream topographic and change detection sections: 1–2 are the topographic cross-sections along the paths from Fig. 12.

FIG. 24 Şoldăneşti downstream field photos (taken 24.03.2019—photo number location is the shown number in Fig. 22).

SfM is an affordable tool for obtaining high-resolution *x,y,z* point clouds (Carrivick et al., 2016), but some external factors can introduce errors that might hinder some types of analysis. The most problematic errors are those related to the geometry of acquisition, through which nonlinear deformations are introduced. These errors are well discussed in the literature and

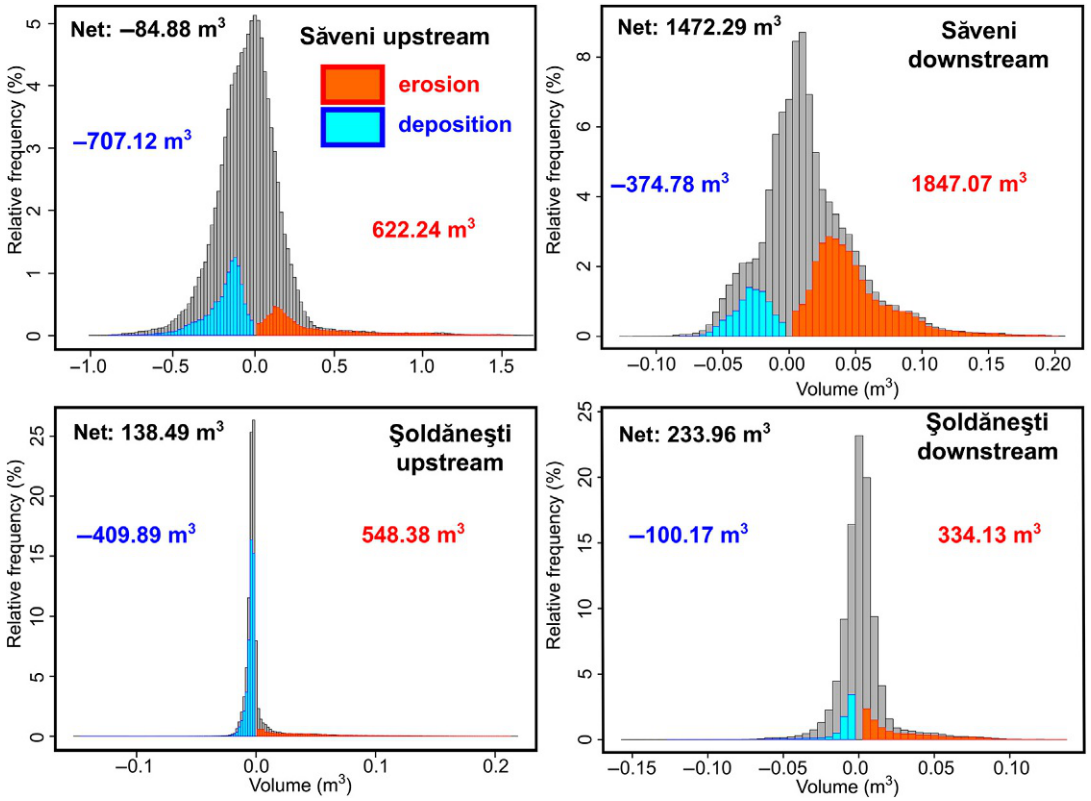

FIG. 25 Histograms of the raw (*gray*) and filtered change detection volumes (*orange* and *blue*) for the four studied gullies.

even guidelines were produced for their minimization (Eltner et al., 2016; Wells et al., 2017; James et al., 2017, 2019). This includes the dishing or doming deformation (Carbonneau and Dietrich, 2017), which in our case has the effect for the GCD by making the gully system to appear either too deep, or too shallow, on the SfM DEM compared with the LiDAR surface. Related to the processes, the effects will be that both erosion and deposition will be either under- or overestimated. The question is, if this deformation is smaller enough in magnitude than the change, in order not to influence it, so that erosion becomes deposition, or vice versa. In our case these deformations were under 25 cm in the gully area, and were removed by the use of GCD. This is visible and can be checked on the topographic sections from Figs. 14, 17, 20, and 23. In these sections it can be seen that the dry vegetation introduces more error than LiDAR and SfM techniques.

GCPs are very important for reducing the acquisition errors (Javernick et al., 2014) and a sufficient number of GCPs with good distributions can overcome the inherent errors and produce good qualitative and quantitative estimations of the rate of change. The photogrammetry success also depends on the image texture (Fonstad et al., 2013).

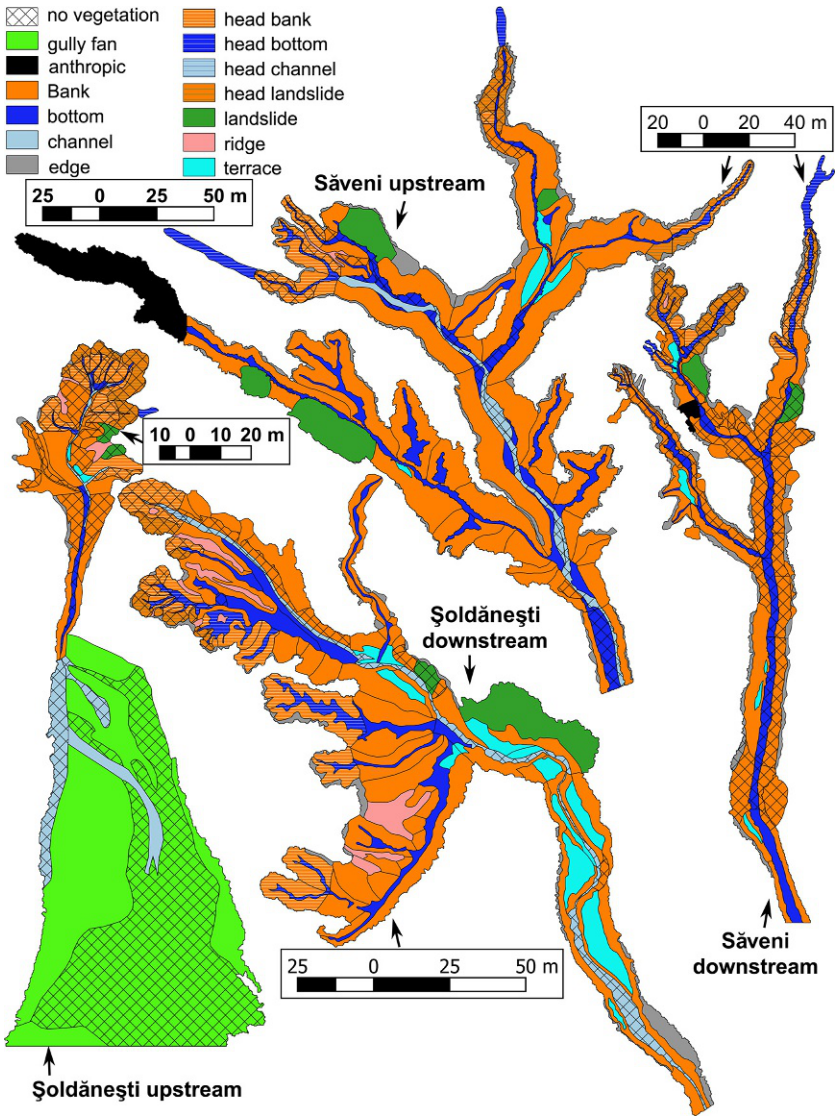

FIG. 26 The geomorphological maps of the studied gullies.

Geomorphological mapping is very important for assessing process rates and for interpreting the detection data of geomorphic change. Even for relatively simple landforms such as gullies, the aerophoto interpretation of the UAV orthoimagery is relevant in deciphering natural or anthropic processes. For example, the gully bottom that is a relatively flat area has a microtopography created by the incised water flow or the deposition of sediment carried by the water flow at higher discharges and by the erosion or landsliding processes that affect the bank. Even the gully bank edge is sometimes very hard to be located,

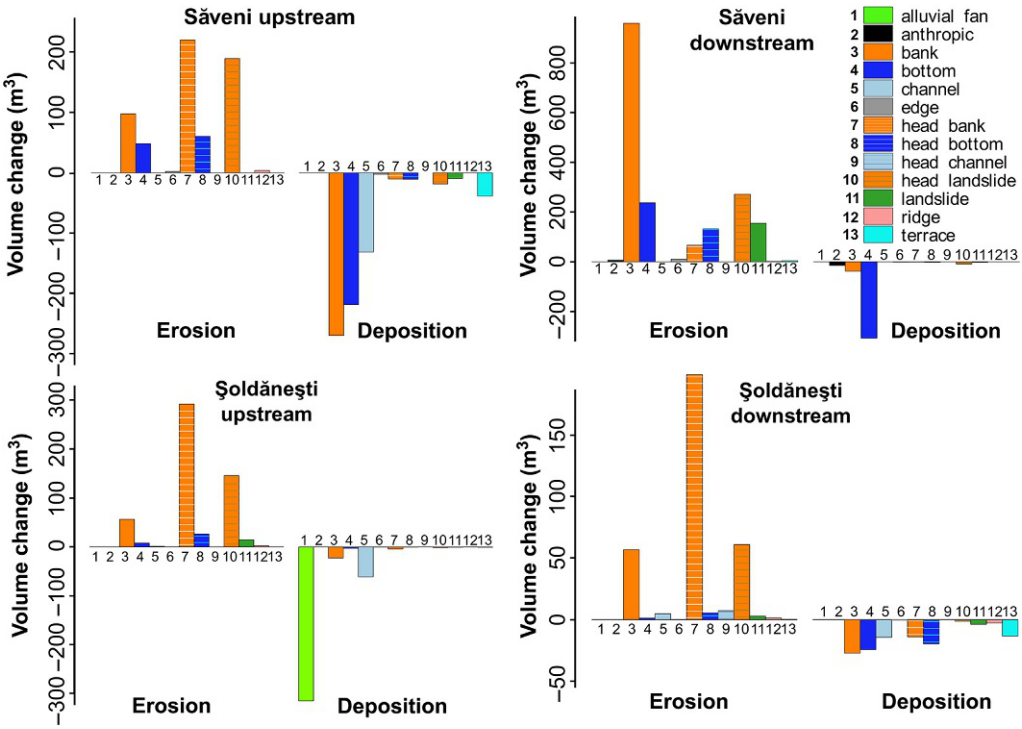

FIG. 27 The balance of change detection volumes for every studied gully by geomorphological unit.

since erosion shapes its hard edges or landsliding or even the multistep evolution of the gully incision is creating multiple morphometric edges (Fig. 8).

The shape of these erosional features makes easier the assessment of positional errors in regard to the two DEMs used for change detection, which is not the case with complicated environments like braided rivers. The presence of erosion on one side, and of deposition on the other side, or of erosion/deposition of the flat areas around the landslide is an indicator of a misalignment, and can be easily found. The presence of water in the gully channel needs the evaluation of the depths through a reflection model (Dietrich, 2017) or other image-enhancing techniques (Partama et al., 2018) to deal with water reflections.

Despite these errors, the application of the complex Wheaton approach is able to filter the changes related to errors in LiDAR and SfM, or due to vegetation, to show the meaningful changes that can be attributed to gully processes (Figs. 13–24). Although the LiDAR and UAV photogrammetry have reasonable accuracy and precision (Tables 1–6), the characteristics of these methods of topographic modeling affect the minimal unit of geomorphological change that can be derived. This can be problematic if we investigate processes with very low process rates or with very dense time frequency, for which the error rate is similar to the process rate, such as, for example, soil erosion (Hänsel et al., 2016).

Geomorphological mapping is a good opportunity to have a check on the field situation in order not to misinterpret the results of the DoD (Kaiser et al., 2018): for example, in the case of

bank landslides, deposition can occur on steep banks, so mapping these landslides and allowing the negative value of raw DoD to pass through uncertainty filtering is an approach that will highlight important processes that otherwise might be filtered out.

6 Conclusions

The new methods of elevation acquisition such as GPS, LiDAR, and SfM are easy-to-use techniques for landform quantification, and their usage opened the possibility of performing analyses of the rate of processes, both in a qualitative and quantitative way. We present such a case, where two different elevation acquisition methods are used to evaluate the rate of process for four reservoir bottom gully systems between two temporal frames.

The big temporal window (2012–19) is overcome by the fact that these gullies evolve slowly mainly during late winter, early spring, or even during summer, during snowmelt or high rainfall events. The DoD approach is able to find and remove errors related to the deformations of the UAV SfM DEM and to the presence of dry vegetation on the LiDAR DEM, and to reveal the changes due to geomorphological processes.

The main gully geomorphological processes were identified and a raw sediment budget was established, although for detailed sediment budgets, denser temporal surveys are needed in order to establish the seasonal evolution. Headwall and headbank erosion are the processes through which these gullies extend. The main branches evolve through channel deepening and widening with important volumes of sediments eroded from the banks and deposited along the channels and the bottoms. Landsliding is an important phenomenon affecting banks, especially in the head areas, which can be mapped and quantified using the DoD approach.

The availability of the LiDAR data for extended areas is a positive factor, because the methods can be used to assess the state of the gully systems in the near past by UAV surveying and SfM DEMs. For further studies, UAV SfM is a promising tool that can be used to monitor the evolution of the gully systems in the near future. Detailed surveys (at least 2 flights per year) are planned for studying the model of evolution of these gullies from NE Romania.

Acknowledgments

This work was supported by a grant of the Ministry of Research and Innovation, CNCS—UEFISCDI, project number PN-III-P1-1.1-PD-2016-0154, within PNCDI III. We are grateful to the Prut-Bârlad Water Administration who provided us the LIDAR data. We have used the computational facilities given by the infrastructure provided through the POSCCE-O 2.2.1, SMIS-CSNR 13984-901, No. 257/28.09.2010 Project, CERNESIM (L4). Silviu Doru, Valeriu Stoilov-Linu, and Georgiana Văculișteanu's help with the fieldwork is highly appreciated.

References

Adams, J.C., Chandler, J.H., 2002. Evaluation of lidar and medium scale photogrammetry for detecting soft-cliff coastal change. Photogramm. Rec. 17 (99), 405–418. https://doi.org/10.1111/0031-868x.00195.

Aschenwald, J., Leichter, K., Tasserand, E., Tappeiner, U., 2001. Spatio-temporal landscape analysis in mountainous terrain by means of small format photography: a methodological approach. IEEE Trans. Geosci. Remote Sens. 39 (4), 885–893. https://doi.org/10.1109/36.917917.

ASPRS, 2004. Guidelines Vertical Accuracy Reporting for Lidar Data. V. 1.0. https://www.asprs.org/a/society/committees/standards/Vertical_Accuracy_Reporting_for_Lidar_Data.pdf.

ASPRS, 2005. LIDAR Guidelines: Horizontal Accuracy Reporting. V. 0.9. https://www.asprs.org/a/society/committees/standards/Horizontal_Accuracy_Reporting_for_Lidar_Data.pdf.

ASPRS, 2018. ASPRS guidelines on geometric inter-swath accuracy and quality of Lidar data. Photogramm. Eng. Remote Sens. 84 (3), 117–128. https://doi.org/10.14358/PERS.84.3.117.

Baltsavias, E.P., 1999. A comparison between photogrammetry and laser scanning. ISPRS J. Photogramm. Remote Sens. 54, 83–94. https://doi.org/10.1016/S0924-2716(99)00014-3.

Baltsavias, E.P., Favey, E., Bauder, A., Bösch, H., Pateraki, M., 2001. Digital surface modelling by airborne laser scanning and digital photogrammetry for glacier monitoring. Photogramm. Rec. 17, 243–273. https://doi.org/10.1111/0031-868X.00182.

Bangen, S., Hensleigh, J., McHugh, P., Wheaton, J.M., 2016. Error modeling of DEMs from topographic surveys of rivers using fuzzy inference systems. Water Resour. Res. 52, 1176–1193. https://doi.org/10.1002/2015WR018299.

Barker, R., Dixon, L., Hooke, J., 1997. Use of terrestrial photogrammetry for monitoring and measuring bank erosion. Earth Surf. Process. Landf. 22 (13), 1217–1227. https://doi.org/10.1002/(SICI)1096-9837(199724)22:13<1217::AID-ESP819>3.0.CO;2-U.

Bergonse, R.V., Reis, E.J., 2011. Theoretical constraints to gully erosion research: time for a re-evaluation of concepts and assumptions? Earth Surf. Process. Landf. 36 (11), 1554–1557. https://doi.org/10.1002/esp.2188.

Bettis III, E.A., Thompson, D.M., 1985. Gully erosion. Rangelands 7 (2), 70–72.

Betts, H.D., DeRose, R.C., 1999. Digital elevation models as a tool for monitoring and measuring gully erosion. Int. J. Appl. Earth Obs. Geoinf. 1, 91–101. https://doi.org/10.1016/S0303-2434(99)85002-8.

Bird, S., Hogan, D., Schwab, J., 2010. Photogrammetric monitoring of small streams under a riparian forest canopy. Earth Surf. Process. Landf. 35 (8), 952–970. https://doi.org/10.1002/esp.2001.

Bocco, G., 1991. Gully erosion: processes and models. Prog. Phys. Geog. 15 (4), 392–406. https://doi.org/10.1177/030913339101500403.

Bocoo, G., Valenzuela, C.R., 1993. Integrating satellite-remote sensing and geographic information systems technologies in gully erosion research. Remote Sens. Rev. 7 (3–4), 233–240. https://doi.org/10.1080/02757259309532179.

Bowen, Z.H., Waltermire, R.G., 2002. Evaluation of light detection and ranging (lidar) for measuring river corridor topography. J. Am. Water Resour. Assoc. 38 (1), 33–41. https://doi.org/10.1111/j.1752-1688.2002.tb01532.x.

Brasington, J., Smart, R.M.A., 2003. Close range digital photogrammetric analysis of experimental drainage basin evolution. Earth Surf. Process. Landf. 28 (3), 231–247. https://doi.org/10.1002/esp.480.

Brasington, J., Vericat, D., Rychkov, I., 2012. Modeling river bed morphology, roughness, and surface sedimentology using high resolution terrestrial laser scanning. Water Resour. Res. 48, W11519.

Cao, W., Sofia, G., Tarolli, P., 2020. Geomorphometric characterisation of natural and anthropogenic land covers. Prog. Earth Planet. Sci. 7, 2. https://doi.org/10.1186/s40645-019-0314-x.

Carbonneau, P.E., Dietrich, J.T., 2017. Cost-effective non-metric photogrammetry from consumer-grade sUAS: implications for direct georeferencing of structure from motion photogrammetry. Earth Surf. Process. Landf. 43 (3), 473–486. https://doi.org/10.1002/esp.4012.

Carrivick, J., Quincey, D., Smith, M., 2016. Structure From Motion in the Geosciences. New Analytical Methods in Earth and Environmental Science. 197, Wiley Blackwell.

Castillo, C., James, M.R., Redel-Macías, M.D., Pérez, R., Gómez, J.A., 2015. SF3M software: 3-D photo-reconstruction for nonexpert users and its application to a gully network. Soil 1, 583–594. https://doi.org/10.5194/soil-1-583-2015.

Castillo, C., Marín-Moreno, V.J., Pérez, R., Muñoz-Salinas, R., Taguas, E.V., 2018. Accurate automated assessment of gully cross-section geometry using the photogrammetric interface FreeXSapp. Earth Surf. Process. Landf. 43 (8), 1726–1736. https://doi.org/10.1002/esp.4341.

Cavalli, M., Tarolli, P., 2011. Application of LiDAR technology for rivers analysis. Ital. J. Eng. Geol. Environ. 1, 33–44. https://doi.org/10.4408/IJEGE.2011-01.S-03.

Cavalli, M., Tarolli, P., Marchi, L., Dalla Fontana, G., 2008. The effectiveness of airborne LiDAR data in the recognition of channel-bed morphology. Catena 73 (3), 249–260. https://doi.org/10.1016/j.catena.2007.11.001.

Chandler, J.H., 1999. Effective application of automated digital photogrammetry for geomorphological research. Earth Surf. Process. Landf. 24 (1), 51–63. https://doi.org/10.1002/(SICI)1096-9837(199901)24:13.0.CO;2-H.

Chandler, J., Ashmore, P., Paola, C., Gooch, M., Varkaris, F., 2003. Monitoring river channel change using terrestrial oblique digital imagery and automated digital photogrammetry. Ann. Assoc. Am. Geogr. 92 (4), 631–644. https://doi.org/10.1111/1467-8306.00308.

Chandler, J.H., Fryer, J.G., Jack, A., 2005. Metric capabilities of low cost digital cameras for close range surface measurement. Photogramm. Rec. 20 (109), 12–26. https://doi.org/10.1111/j.1477-9730.2005.00302.x.

Chen, J., Li, K., Chang, K.-J., Sofia, G., Tarolli, P., 2015. Open-pit mining geomorphic feature characterization. Int. J. Appl. Earth Obs. Geoinf. 42, 76–86. https://doi.org/10.1016/j.jag.2015.05.001.

Clarke, T.A., Fryer, J.G., 1998. The development of camera calibration methods and models. Photogramm. Rec. 16 (91), 51–66. https://doi.org/10.1111/0031-868X.00113.

Colomina, I., Molina, P., 2014. Unmanned aerial systems for photogrammetry and remote sensing: a review. ISPRS J. Photogramm. Remote Sens. 92, 79–97. https://doi.org/10.1016/j.isprsjprs.2014.02.013.

Conrad, O., Bechtel, B., Bock, M., Dietrich, H., Fischer, E., Gerlitz, L., Wehberg, J., Wichmann, V., Böhner, J., 2015. System for automated geoscientific analyses (SAGA) v. 2.1.4. Geosci. Model Dev. 8, 1991–2007. https://doi.org/10.5194/gmd-8-1991-2015.

Cucchiaro, S., Cavalli, M., Vericat, D., Crema, S., Llena, M., Beinat, A., Marchi, L., Cazorzi, F., 2018. Monitoring topographic changes through 4D-structure-from-motion photogrammetry: application to a debris-flow channel. Environ. Earth Sci. 77, 632. https://doi.org/10.1007/s12665-018-7817-4.

Derron, M.-H., Jaboyedoff, M., 2010. Preface "LIDAR and DEM techniques for landslides monitoring and characterization" Nat. Hazards Earth Syst. Sci. 10, 1877–1879. https://doi.org/10.5194/nhess-10-1877-2010.

Dewitte, O., Jasselette, J.-C., Cornet, Y., Van Den Eeckhaut, M., Collignon, A., Poesen, J., Demoulin, A., 2008. Tracking landslide displacements by multi-temporal DTMs: a combined aerial stereophotogrammetric and LIDAR approach in western Belgium. Eng. Geol. 99 (1–2), 11–22. https://doi.org/10.1016/j.enggeo.2008.02.006.

Di Stefano, C., Ferro, V., Palmeri, V., Pampalone, V., 2017. Testing the use of an image-based technique to measure gully erosion at Sparacia experimental area. Hydrol. Process. 31 (3), 573–585. https://doi.org/10.1002/hyp.11048.

Di Stefano, C., Palmeri, V., Pampalone, V., 2019. An automatic approach for rill network extraction to measure rill erosion by terrestrial and low-cost UAV photogrammetry. Hydrol. Process. 33 (13), 1883–1895. https://doi.org/10.1002/hyp.13444.

Dietrich, J.T., 2017. Bathymetric Structure-from-Motion: extracting shallow stream bathymetry from multi-view stereophotogrammetry. Earth Surf. Process. Landf. 42 (2), 355–364. https://doi.org/10.1002/esp.4060.

Eltner, A., Baumgart, P., 2015. Accuracy constraints of terrestrial Lidar data for soil erosion measurement: application to a Mediterranean field plot. Geomorphology 245, 243–254. https://doi.org/10.1016/j.geomorph.2015.06.008.

Eltner, A., Mulsow, C., Maas, H.-G., 2013. Quantitative measurement of soil erosion from TLS and UAV data. Int. Arch. Photogramm. Remote Sens. Spat. Inf. Sci. XL-1/W2, 119–124. https://doi.org/10.5194/isprsarchives-XL-1-W2-119-2013.

Eltner, A., Baumgart, P., Maas, H.-G., Faust, D., 2015. Multi-temporal UAV data for automatic measurement of rill and interrill erosion on loess soil. Earth Surf. Process. Landf. 40 (6), 741–755. https://doi.org/10.1002/esp.3673.

Eltner, A., Kaiser, A., Castillo, C., Rock, G., Neugirg, F., Abellán, A., 2016. Image-based surface reconstruction in geomorphometry—merits, limits and developments. Earth Surf. Dyn. 4, 359–389. https://doi.org/10.5194/esurf-4-359-2016.

Eltner, A., Kaiser, A., Abellan, A., Schindewolf, M., 2017. Time lapse structure-from-motion photogrammetry for continuous geomorphic monitoring. Earth Surf. Process. Landf. 42 (14), 2240–2253. https://doi.org/10.1002/esp.4178.

Ely, J.C., Graham, C., Barr, I.D., Rea, B.R., Spagnolo, M., Evans, J., 2016. Using UAV acquired photography and structure from motion techniques for studying glacier landforms: application to the glacial flutes at Isfallsglaciären. Earth Surf. Process. Landf. 42 (6), 877–888. https://doi.org/10.1002/esp.4044.

Evans, J.S., Hudak, A.T., 2007. A multiscale curvature algorithm for classifying discrete return LiDAR in forested environments. IEEE Trans. Geosci. Remote Sens. 45 (4), 1029–1038. https://doi.org/10.1109/TGRS.2006.890412.

Evans, M., Lindsay, J.B., 2010. High resolution quantification of gully erosion in upland peatlands at the landscape scale. Earth Surf. Process. Landf. 35 (8), 876–886. https://doi.org/10.1002/esp.1918.

Falkner, E., Morgan, D., 2002. Aerial Mapping. Methods and Applications, second ed. CRC Press, Boca Raton.

Farres, P., Poesen, J., Wood, S., 1993. Soil erosion landscapes. Geogr. Rev. 6, 38–41.

Fischler, M.A., Bolles, R.C., 1981. Random sample consensus: a paradigm for model fitting with applications to image analysis and automated cartography. Commun. ACM CACM 24 (6), 381–395. https://doi.org/10.1145/358669.358692.

Fonstad, M.A., Dietrich, J.T., Courville, B.C., Jensen, J.L., Carbonneau, P.E., 2013. Topographic structure from motion: a new development in photogrammetric measurement. Earth Surf. Process. Landf. 38 (4), 421–430. https://doi.org/10.1002/esp.3366.

Frankl, A., Stal, C., Abraha, A., Nyssen, J., Rieke-Zapp, D., De Wulf, A., Poesen, J., 2015. Detailed recording of gully morphology in 3D through image-based modelling. Catena 127, 92–101. https://doi.org/10.1016/j.catena.2014.12.016.

Fraser, C.S., Cronk, S., 2009. A hybrid measurement approach for close-range photogrammetry. ISPRS J. Photogramm. Remote Sens. 64 (3), 328–333. https://doi.org/10.1016/j.isprsjprs.2008.09.009.

Furukawa, Y., Ponce, J., 2007. Accurate, dense, and robust multi-view stereopsis. In: IEEE Computer Society Conference on Computer Vision and Pattern Recognition (CVPR 2007) 1, pp. 1–8. https://doi.org/10.1109/CVPR.2007.383246.

Furukawa, Y., Ponce, J., 2010. Accurate, dense, and robust multi-view stereopsis. IEEE Trans. Pattern Anal. Mach. Intell. 32 (8), 1362–1376. https://doi.org/10.1109/TPAMI.2009.161.

Furukawa, Y., Curless, B., Seitz, S.M., Szeliski, R., 2010. Towards Internet-scale multi-view stereo. In: 2010 IEEE Computer Society Conference on Computer Vision and Pattern Recognition 1–8, 13–18 June 2010, San Francisco, CA, USAhttps://doi.org/10.1109/CVPR.2010.5539802.

Garibaldi, J., Chen, C., Razak, T., 2017. FuzzyR: Fuzzy Logic Toolkit for R. R package version 2.1. https://CRAN.R-project.org/package=FuzzyR.

Gesch, K.R., Wells, R.R., Cruise, R.M., Momm, H.G., Dabney, S.M., 2015. Quantifying uncertainty of measuring gully morphological evolution with close-range digital photogrammetry. Soil Sci. Soc. Am. J. 79 (2), 650–659. https://doi.org/10.2136/sssaj2014.10.0396.

Geyik, M.P., 1986. FAO watershed management field manual. Gully Control. FAO Conservation guide 13/2 Rome.

Giménez, R., Marzolff, I., Campo, M.A., Seeger, M., Ries, J.B., Casalí, J., Álvarez-Mozos, J., 2009. Accuracy of high-resolution photogrammetric measurements of gullies with contrasting morphology. Earth Surf. Process. Landf. 34 (14), 1915–1926. https://doi.org/10.1002/esp.1868.

Giordan, D., Nex, F.C., Hayakawa, Y., Remondino, F., Tarolli, P., 2018. The use of remotely piloted aircraft systems (RPASs) for natural hazards monitoring and management. Nat. Hazards Earth Syst. Sci. 18, 1079–1096. https://doi.org/10.5194/nhess-18-1079-2018.

Glendell, M., McShane, G., Farrow, L., James, M.R., Quinton, J., Anderson, K., Evans, M., Benaud, P., Rawlins, B., Morgan, D., Jones, L., Kirkham, M., DeBell, L., Quine, T.A., Lark, M., Rickson, J., Brazier, R.E., 2017. Testing the utility of structure-from-motion photogrammetry reconstructions using small unmanned aerial vehicles and ground photography to estimate the extent of upland soil erosion. Earth Surf. Process. Landf. 42 (12), 1860–1871. https://doi.org/10.1002/esp.4142.

Gómez-Gutiérrez, A., Schnabel, S., Berenguer-Sempere, F., Lavado- Contador, F., Rubio-Delgado, J., 2014. Using 3D photo-reconstruction methods to estimate gully headcut erosion. Catena 120, 91–101. https://doi.org/10.1016/j.catena.2014.04.004.

Gong, C., Lei, S., Bian, Z., Liu, Y., Zhang, Z., Cheng, W., 2019. Analysis of the development of an erosion gully in an open-pit coal mine dump during a winter freeze-thaw cycle by using low-cost UAVs. Remote Sens. 11, 1356. https://doi.org/10.3390/rs11111356.

Guzzetti, F., Mondini, A.C., Cardinali, M., Fiorucci, F., Santangelo, M., Chang, K.-T., 2012. Landslide inventory map: new tools for an old problem. Earth Sci. Rev. 112, 42–66. https://doi.org/10.1016/j.earscirev.2012.02.001.

Haas, F., Heckmann, T., Hilger, L., Becht, M., 2012. Quantification and modelling of debris flows in the proglacial area of the Gepatschferner, Austria, using ground-based LiDAR. In: Erosion and Sediment Yields in the Changing Environment, Proceedings of a Symposium held at the Institute of Mountain Hazards and Environment, CAS-Chengdu, China, 11–15 October 2012, pp. 293–302. IAHS Publication no. 356.

Hamshaw, S.D., Bryce, T., Rizzo, D.M., O'Neil-Dunne, J., Frolik, J., Dewoolkar, M.M., 2017. Quantifying streambank movement and topography using unmanned aircraft system photogrammetry with comparison to terrestrial laser scanning. River Res. Appl. 33 (8), 1354–1367. https://doi.org/10.1002/rra.3183.

Hancock, G.R., Willgoose, G.R., 2001. The production of digital elevation models for experimental model landscapes. Earth Surf. Process. Landf. 26 (5), 475–490. https://doi.org/10.1002/esp.187.

Haneberg, W.C., 2008. Using close range terrestrial digital photogrammetry for 3-D rock slope modeling and discontinuity mapping in the United States. Bull. Eng. Geol. Environ. 67 (4), 457–469. https://doi.org/10.1007/s10064-008-0157-y.

Hänsel, P., Schindewolf, M., Eltner, A., Kaiser, A., Schmidt, J., 2016. Feasibility of high-resolution soil erosion measurements by means of rainfall simulations and SfM photogrammetry. Hydrology 3 (38), 16. https://doi.org/10.3390/hydrology3040038.

Harpold, A.A., Marshall, J.A., Lyon, S.W., Barnhart, T.B., Fisher, B.A., Donovan, M., Brubaker, K.M., Crosby, C.J., Glenn, N.F., Glennie, C.L., Kirchner, P.B., Lam, N., Mankoff, K.D., McCreight, J.L., Molotch, N.P., Musselman, K.N., Pelletier, J., Russo, T., Sangireddy, H., Sjöberg, Y., Swetnam, T., West, N., 2015. Laser vision: lidar as a transformative tool to advance critical zone science. Hydrol. Earth Syst. Sci. 19, 2881–2897. https://doi.org/10.5194/hess-19-2881-2015.

Heede, B.H., 1976. Gully Development and Control: The Status of Our Knowledge. USDA Forest Service Research Paper RM-169, Rocky Mountain Forest and Range Experiment Station, Forest Service, U.S. Department of Agriculture, Fort Collins, Colorado 80521.

Heimsath, A.M., Farid, H., 2002. Hillslope topography from unconstrained photographs. Math. Geol. 34 (8), 929–952. https://doi.org/10.1023/A:1021364623017.

Heng, B.C.P., Chandler, J.H., Armstrong, A., 2010. Applying close-range digital photogrammetry and soil erosion studies. Photogramm. Rec. 25 (131), 240–265. https://doi.org/10.1111/j.1477-9730.2010.00584.x.

Hengl, T., 2006. Finding the right pixel size. Comput. Geosci. 32 (9), 1283–1298. https://doi.org/10.1016/j.cageo.2005.11.008.

Heritage, G.L., Fuller, I.C., Charlton, M.E., Brewer, P.A., Passmore, D.P., 1999. CDW photogrammetry of low relief fluvial features: accuracy and implications for reach-scale sediment budgeting. Earth Surf. Process. Landf. 23 (13), 1219–1233. https://doi.org/10.1002/(SICI)1096-9837(199812)23:13<1219::AID-ESP927>3.0.CO;2-R.

Heritage, G.L., Milan, D.J., Large, A.R.G., Fuller, I.C., 2009. Influence of survey strategy and interpolation model on DEM quality. Geomorphology 112, 334–344. https://doi.org/10.1016/j.geomorph.2009.06.024.

Hickman, G.D., Hogg, J.E., 1969. Application of an airborne pulsed laser for near shore bathymetric measurements. Remote Sens. Environ. 1 (1), 47–58. https://doi.org/10.1016/s0034-4257(69)90088-1.

Hijmans, R.J., 2017. Raster: Geographic Data Analysis and Modeling. R package version 2. 6–7. https://CRAN.R-project.org/package=raster.

Hodgson, M.E., Bresnahan, P., 2004. Accuracy of airborne Lidar-derived elevation: empirical assessment and error budget. Photogram. Eng. Remote Sens. 70, 331–339. https://doi.org/10.14358/PERS.70.3.331.

Imeson, A.C., Kwaad, F.J.P.M., 1980. Gully types and gully prediction. Geografisch Tijdschrift 14 (5), 430–441.

Inkpen, R., 2018. New technologies and the political economy of geomorphology. Can. Geogr. 62, 1–12. https://doi.org/10.1111/cag.12455.

Ireland, H.A., Sharpe, C.F.S., Eargle, D.H., 1939. Principles of Gully Erosion in the Piedmont of South Carolina. Technical Bulletin No. 633. U.S. Department of Agriculture, Washington, DC, pp. 1–143.

Irish, J.L., White, T.E., 1998. Coastal engineering applications of high-resolution lidar bathymetry. Coast. Eng. 35 (1–2), 47–71. https://doi.org/10.1016/s0378-3839(98)00022-2.

Jaboyedoff, M., Oppikofer, T., Abellán, A., Derron, M.-H., Loye, A., Metzger, R., Pedrazzini, A., 2012. Use of lidar in landslide investigations: a review. Nat. Hazards 61, 5–28. https://doi.org/10.1007/s11069-010-9634-2.

James, M.R., Robson, S., 2012. Straightforward reconstruction of 3-D surfaces and topography with a camera: accuracy and geoscience application. J. Geophys. Res. 117, F03017. https://doi.org/10.1029/2011JF002289.

James, M.R., Robson, S., 2014. Mitigating systematic error in topographic models derived from UAV and ground-based image networks. Earth Surf. Process. Landf. 39 (10), 1413–1420. https://doi.org/10.1002/esp.3609.

James, A., Watson, D.G., Hansen, W.F., 2007. Using LIDAR data to map gullies and headwater streams under forest canopy: South Carolina, USA. Catena 71 (1), 132–144. https://doi.org/10.1016/j.catena.2006.10.010.

James, M.R., Robson, S., Smith, M.W., 2017. 3-D uncertainty-based topographic change detection with structure-from-motion photogrammetry: precision maps for ground control and directly georeferenced surveys. Earth Surf. Process. Landf. 42 (12), 1769–1788. https://doi.org/10.1002/esp.4125.

James, M.R., Chandler, J.H., Eltner, A., Fraser, C., Miller, P.E., Mills, J.P., Noble, T., Robson, S., Lane, S.N., 2019. Guidelines on the use of structure-from-motion photogrammetry in geomorphic research. Earth Surf. Process. Landf. 44, 2081–2084. https://doi.org/10.1002/esp.4637.

Javernick, L., Brasington, J., Caruso, B., 2014. Modeling the topography of shallow braided rivers using Structure-from-Motion photogrammetry. Geomorphology 213, 166–182. https://doi.org/10.1016/j.geomorph.2014.01.006.

Kaiser, A., Neugirg, F., Rock, G., Müller, C., Haas, F., Ries, J.B., Schmidt, J., 2014. Small-scale surface reconstruction and volume calculation of soil erosion in complex Moroccan gully morphology using structure from motion. Remote Sens. 6, 7050–7080. https://doi.org/10.3390/rs6087050.

Kaiser, A., Erhardt, A., Eltner, A., 2018. Addressing uncertainties in interpreting soil surface changes by multi-temporal high resolution topography data across scales. Land Degrad. Dev. 29 (8), 2264–2277. https://doi.org/10.1002/ldr.2967.

Keutterling, A., Thomas, A., 2006. Monitoring glacier elevation and volume changes with digital photogrammetry and GIS at Gepatschferner glacier, Austria. Int. J. Remote Sens. 27, 4371–4380. https://doi.org/10.1080/01431160600851819.

Koci, J., Jarihani, B., Leon, J.X., Sidle, R.C., Wilkinson, S.N., Bartley, R., 2017. Assessment of UAV and ground-based structure from motion with multi-view stereo photogrammetry in a gullied savanna catchment. ISPRS Int. J. Geo Inf. 6 (328), 23. https://doi.org/10.3390/ijgi6110328.

Krosley, L.K., Shaffner, P.T., Oerter, E., Ortiz, T., 2006. Digital ground-based photogrammetry for measuring discontinuity orientations in steep rock exposures. In: Proceedings of the 41st U.S. Symposium of Rock Mechanics (USRMS), 17–21 June, Golden, Colorado, pp. 1–13.

Lane, S.N., 2000. The measurement of river channel morphology using digital photogrammetry. Photogramm. Rec. 16 (96), 937–961. https://doi.org/10.1111/0031-868X.00159.

Lane, S.N., James, T.D., Crowell, M.D., 2000. Application of digital photogrammetry to complex topography for geomorphological research. Photogramm. Rec. 16 (95), 793–821. https://doi.org/10.1111/0031-868X.00152.

Lane, S.N., Chandler, J.H., Porfiri, K., 2001. Monitoring river channel and flume surfaces with digital photogrammetry. J. Hydraul. Eng. 127 (10), 871–877. https://doi.org/10.1061/(ASCE)0733-9429(2001)127:10(871).

Lannoeye, W., Stal, C., Guyassa, E., Zenebe, A., Nyssen, J., Frankl, A., 2016. The use of SfM-photogrammetry to quantify and understand gully degradation at the temporal scale of rainfall events: an example from the Ethiopian drylands. Phys. Geogr. 37 (6), 430–451. https://doi.org/10.1080/02723646.2016.1234197.

Lee, S.J., Wolberg, G., Shin, S., 1997. Scattered data interpolation with multilevel B-splines. IEEE Trans. Vis. Comput. Graph. 3 (3), 228–244. https://doi.org/10.1109/2945.620490.

Leopold, L.B., Miller, J.P., 1956. Ephemeral streams. Hydraulic factors and their relation to the drainage net. US Geological Survey PP 282-A.

Li, J., Li, E., Chen, Y., Xu, L., Zhang, Y., 2010. Bundled depth-map merging for multi-view stereo. In: 2010 IEEE Computer Society Conference on Computer Vision and Pattern Recognition (CVPR), June 13–18, 2010, pp. 2769–2776. San Francisco, CAhttps://doi.org/10.1109/CVPR.2010.5540004.

Lin, C.W., Tseng, C.-M., Tseng, Y.-H., Fei, L.-Y., Hsieh, Y.-C., Tarolli, P., 2013. Recognition of large scale deep-seated landslides in forest areas of Taiwan using high resolution topography. J. Asian Earth Sci. 62, 389–400. https://doi.org/10.1016/j.jseaes.2012.10.022.

Linder, W., 2016. Digital Photogrammetry. A Practical Course. Springer Berlin Heidelberg. https://doi.org/10.1007/978-3-662-50463-5.

Liu, X., 2008. Airborne LiDAR for DEM generation: some critical issues. Prog. Phys. Geogr. 32 (1), 31–49. https://doi.org/10.1177/0309133308089496.

Liu, K., Ding, H., Tang, G., Na, J., Huang, X., Xue, Z., Yang, X., Li, F., 2016. Detection of catchment-scale gully-affected areas using unmanned aerial vehicle (UAV) on the Chinese Loess Plateau. ISPRS Int. J. Geo-Inf. 5 (238), 21. https://doi.org/10.3390/ijgi5120238.

Liu, C., Shao, X., Wu, H., Li, N., Qu, T., Dotta, G., Huang, Y., 2018. Giant landslide displacement analysis using a point cloud set conflict technique: a case in Xishancun landslide, Sichuan, China. Int. J. Remote Sens. 40, 3247–3266. https://doi.org/10.1080/01431161.2018.1541331.

Lloyd, C.D., Atkinson, P.M., 2002. Deriving DSMs from lidar data with kriging. Int. J. Remote Sens. 23 (12), 2519–2524. https://doi.org/10.1080/01431160110097998.

Longuet-Higgins, H.C., 1981. A computer algorithm for reconstructing a scene from two projections. Nature 293, 133–135. https://doi.org/10.1038/293133a0.

Lowe, D.G., 1999. Object recognition from local scale-invariant features. In: Proceedings of the Seventh IEEE International Conference on Computer Vision, September 20–27, 1999, pp. 1150–1157, Corfu, Greece. https://doi.org/10.1109/ICCV.1999.790410.

Lowe, D.G., 2001. Local feature view clustering for 3D object recognition. In: Proceedings of the 2001 IEEE Computer Society Conference on Computer Vision and Pattern Recognition, CVPR 2001, 8–14 December 2001, 7 pp, Kauai, Hawaii. https://doi.org/10.1109/CVPR.2001.990541.

Lowe, D.G., 2004. Distinctive image features from scale-invariant keypoints. Int. J. Comput. Vis. 60, 91–110. https://doi.org/10.1023/B:VISI.0000029664.99615.94.

Mărgărint, M.C., Niculiță, M., 2016. Using high resolution LIDAR DEM to reconstruct historical network of lakes and wetlands in the Northern part of the Moldavian Plateau, NE Romania. Georeview 26 (2), 59. https://doi.org/10.4316/GEOREVIEW.2016.0.0.336.

Mărgărint, M.C., Niculiță, M., Nemeth, A., Cristea, I., 2017a. Topographic and depositional signature of old anthropic lakes in northern part of the Moldavian Plateau (NE Romania). In: 19th EGU General Assembly, EGU2017, 23–28 April, 2017 in Vienna, Austria, p. 12206. 2017EGUGA..1912206C.

Mărgărint, M.C., Niculiță, M., Doru, S., Necula, N., Cristea, I., 2017b. Old anthropic dams, lacustrine deposits, and gullies from Șoldănești village. In: Niculiță, M., Mărgărint, M.C. (Eds.), Proceedings of Romanian Geomorphology Symposium. In: vol. 1. Alexandru Ioan Cuza University of Iaşi Press, Iași, pp. 137–141. https://doi.org/10.15551/prgs.2017.133.

Marzolff, I., Poesen, J., 2009. The potential of 3D gully monitoring with GIS using high-resolution aerial photography and a digital photogrammetry system. Geomorphology 111 (1–2), 48–60. https://doi.org/10.1016/j.geomorph.2008.05.047.

Marzolff, I., Ries, J.B., Poesen, J., 2011. Short-term versus medium-term monitoring for detecting gully-erosion variability in a Mediterranean environment. Earth Surf. Process. Landf. 36 (12), 1604–1623. https://doi.org/10.1002/esp.2172.

Matthews, N.A., 2008. Aerial and Close-Range Photogrammetry Technology: Providing Resource Documentation, Interpretation, and Preservation. Technical Note 428, U.S. Department of the Interior, Bureau of Land Management, National Operations Center, Denver, Colorado. 42 pp.

McKean, J., Roering, J., 2004. Objective landslide detection and surface morphology mapping using high-resolution airborne laser altimetry. Geomorphology 57 (3–4), 331–351. https://doi.org/10.1016/S0169-555X(03)00164-8.

Micusik, B., Kosecka, J., 2009. Piecewise planar city 3D modeling from street view panoramic sequences. In: 2009 IEEE Conference on Computer Vision and Pattern Recognition (CVPR 2009), June 20–25, 2009, pp. 2906–2912. Miami, FL. https://doi.org/10.1109/CVPR.2009.5206535.

Momm, H.G., Bingner, R., Wells, R., Dabney, S., 2011. Methods for gully characterization in agricultural croplands using ground-based light detection and ranging. In: Bhuiyan, F. (Ed.), Sediment Transport—Flow and Morphological Processes. IntechOpen, pp. 101–124. https://doi.org/10.5772/21360.

Momm, H.G., Bingner, R.L., Wells, R.R., Dabney, S.M., Frees, L.D., 2013. Effect of terrestrial LiDAR point sampling density in ephemeral gully characterization. Open J. Mod. Hydrol. 3, 38–49. https://doi.org/10.4236/ojmh.2013.31006.

Momm, H.G., Wells, R.R., Benett, S.J., 2017. Disaggregating soil erosion processes within an evolving experimental landscape. Earth Surf. Process. Landf. 43 (2), 543–552. https://doi.org/10.1002/esp.4268.

Nagasaka, A., Yanai, S., Sato, H., Hasegawa, S., 2005. Soil erosion and gully growth associated with cultivation in southwestern Hokkaido, Japan. Ecol. Eng. 24, 503–508. https://doi.org/10.1016/j.ecoleng.2005.01.008.

Niculiță, M., 2012. Realizarea unui cadru de lucru pentru analiza geomorfometrică a reliefului reprezentat pe modelele numerice ale suprafeţei terenului (A framework for geomorphometric analysis of landforms from DEMs). Unpublished PhD, Alexandru Ioan Cuza University of Iasi, Iasi, 211 pp. Available at: http://www.geomorphologyonline.com/teza_doctorat_Mihai_Niculita_2012_Analiza_geomorfometrica_a_reliefului.pdf (in Romanian).

Niculiţă, M., 2016. Automatic landslide length and width estimation based on the geometric processing of the bounding box and the geomorphometric analysis of DEMs. Nat. Hazards Earth Syst. Sci. 16, 2021–2030. https://doi.org/10.5194/nhess-16-2021-2016.

Niculiță, M., Mărgărint, M.C., Santangelo, M., 2016. Archaeological evidence for Holocene landslide activity in the eastern Carpathian lowland. Quat. Int. 2016 (415), 175–189. https://doi.org/10.1016/j.quaint.2015.12.048.

Niculiță, M., Mărgărint, M.C., Tarolli, P., 2017. Historical reservoir construction: potential hotspot of anthropogenic induced sediments in lowland Northeastern Romania. In: 19th EGU General Assembly, EGU2017, 23–28 April, 2017 in Vienna, Austria, p. 11922. EGU2017-11922-1.

Nistér, D., 2004. An efficient solution to the five-point relative pose problem. IEEE Trans. Pattern Anal. Mach. Intell. 26, 756–777. https://doi.org/10.1109/TPAMI.2004.17.

Notebaert, B., Verstraeten, G., Govers, G., Poesen, J., 2009. Qualitative and quantitative applications of lidar imagery in fluvial geomorphology. Earth Surf. Process. Landf. 34 (2), 217–231. https://doi.org/10.1002/esp.1705.

Orlandini, S., Tarolli, P., Moretti, G., Dalla Fontana, G., 2011. On the prediction of channel heads in a complex alpine terrain using gridded elevation data. Water Resour. Res. 47, 1–12. https://doi.org/10.1029/2010WR009648.

Partama, I.G.D.Y., Kanno, A., Ueda, M., Akamatsu, Y., Inui, R., Sekine, M., Yamamoto, K., Imai, T., Higuchi, T., 2018. Removal of water-surface reflection effects with a temporal minimum filter for UAV-based shallow-water photogrammetry. Earth Surf. Process. Landf. 43 (12), 2673–2682. https://doi.org/10.1002/esp.4399.

Passalacqua, P., Tarolli, P., Foufoula-Georgiou, E., 2010. Testing space-scale methodologies for automatic geomorphic feature extraction from lidar in a complex mountainous landscape. Water Resour. Res. 46 (1), 1–17. https://doi.org/10.1029/2009WR008812.

Passalacqua, P., Belmont, P., Staley, D.M., Simley, J.D., Arrowsmith, R., Bode, C.A., Crosby, C., DeLong, S.B., Glenn, N.F., Kelly, S.A., Lague, D., Sangireddy, H., Schaffrath, K., Tarboton, D.G., Wasklewicz, T., Wheaton, J.M., 2015. Analyzing high resolution topography for advancing the understanding of mass and energy transfer through landscapes: a review. Earth Sci. Rev. 148, 174–193. https://doi.org/10.1016/j.earscirev.2015.05.012.

Penna, D., Borga, M., Aronica, G.T., Brigandì, G., Tarolli, P., 2014. Predictive power of a shallow landslide model in a high-resolution landscape: dissecting the effects of forest roads. Hydrol. Earth Syst. Sci. 18, 2127–2139. https://doi.org/10.5194/hess-18-2127-2014.

Peppa, M.V., Mills, J.P., Moore, P., Miller, P.E., Chambers, J.E., 2018. Automated co-registration and calibration in SfM photogrammetry for landslide change detection. Earth Surf. Process. Landf. 44 (1), 287–303. https://doi.org/10.1002/esp.4502.

Perroy, R.L., Bookhagen, B., Asner, G.P., Chadwick, O.A., 2010. Comparison of gully erosion estimates using airborne and ground-based LiDAR on Santa Cruz Island, California. Geomorphology 118 (3–4), 288–300. https://doi.org/10.1016/j.geomorph.2010.01.009.

Peter, K.D., d'Oleire-Oltmanns, S., Ries, J.B., Marzolff, I., Ait Hssaine, A., 2014. Soil erosion in gully catchments affected by land-levelling measures in the Souss Basin, Morocco, analysed by rainfall simulation and UAV remote sensing data. Catena 113, 24–40. https://doi.org/10.1016/j.catena.2013.09.004.

Piegay, H., Kondolf, G.M., Minear, J.T., Vaudor, L., 2015. Trends in publications in fluvial geomorphology over two decades: a truly new era in the discipline owing to recent technological evolution? Geomorphology 248, 489–500. https://doi.org/10.1016/j.geomorph.2015.07.039.

Piermattei, L., Carturan, L., de Blasi, F., Tarolli, P., Dalla Fontana, G., Vettore, A., Pfeifer, N., 2016. Suitability of ground-based SfMMVS for monitoring glacial and periglacial processes, Earth Surf. Dyn. 4, 425–443. https://doi.org/10.5194/esurf-4-425-2016

Pijl, A., Bailly, J.S., Feurer, D., Maaoui, M.A.E., Boussema, M.R., Tarolli, P., 2020. TERRA: terrain extraction from elevation Rasters through repetitive anisotropic filtering. Int. J. Appl. Earth Obs. Geoinf. 84, 101977. https://doi.org/10.1016/j.jag.2019.101977.

Poesen, J., Vandaele, K., Van Wesemael, B., 1996. Contribution of gully erosion to sediment production on cultivated lands and rangelands. In: Erosion and Sediment Yield: Global and Regional Perspectives, Proceedings of the Exeter Symposium, July 1996, IAHS Publication No. 236, pp. 251–266.

Poesen, J., Vandaele, K., van Wesemael, B., 1998. Gully Erosion: importance and model implications. In: Boardman, J., Favis-Mortlock, D. (Eds.), Modelling Soil Erosion by Water. In: NATO ASI Series (Series I: Global Environmental Change), vol. 55. Springer, Berlin, Heidelberghttps://doi.org/10.1007/978-3-642-58913-3_22.

Poesen, J., Nachtergaele, J., Verstraten, G., Valentin, C., 2003. Gully erosion and environmental change: importance and research needs. Catena 50, 91–133. https://doi.org/10.1016/S0341-8162(02)00143-1.

Poesen, J., Vanwalleghem, T., de Vente, J., Knapen, A., Verstraeten, G., Martínez-Casasnovas, J.A., 2006. Gully erosion in Europe, in Soil Erosion in Europe, J. Boardman and J. Poesen (eds.), Wiley, 515–536.

Prosdocimi, M., Calligaro, S., Sofia, G., Dalla Fontana, G., Tarolli, P., 2015. Bank erosion in agricultural drainage networks: new challenges from structure-from-motion photogrammetry for post-event analysis. Earth Surf. Process. Landf. 40 (14), 1891–1906. https://doi.org/10.1002/esp.3767.

Prosdocimi, M., Burguet, M., Di Prima, S., Sofia, G., Terol, E., Rodrigo Comino, J., Cerdà, A., Tarolli, P., 2017. Rainfall simulation and Structure-from-Motion photogrammetry for the analysis of soil water erosion in Mediterranean vineyards. Sci. Total Environ. 574, 204–215. https://doi.org/10.1016/j.scitotenv.2016.09.036.

Pyle, C.J., Richards, K.S., Chandler, J.H., 1997. Digital photogrammetric monitoring of river bank erosion. Photogramm. Rec. 15 (89), 753–764. https://doi.org/10.1111/0031-868X.00083.

Qin, C., Wells, R.R., Momm, H.G., Zu, X., Wilson, G.V., Zheng, F., 2019. Photogrammetric analysis tools for channel widening quantification under laboratory conditions. Soil Tillage Res. 191, 306–316. https://doi.org/10.1016/j.still.2019.04.002.

R Core Team, 2013. R: A language and Environment for Statistical Computing. R Foundation for Statistical Computing, Vienna, Austria. ISBN 3-900051-07-0. http://www.R-project.org/.

Remondino, F., El-Hakim, S., 2006. Image-based 3D modelling: a review. Photogramm. Rec. 21 (15), 269–291. https://doi.org/10.1111/j.1477-9730.2006.00383.x.

Rieke-Zapp, D.H., Nearing, M.A., 2005. Digital close range photogrammetry for measurement of soil erosion. Photogramm. Rec. 20 (109), 69–87. https://doi.org/10.1111/j.1477-9730.2005.00305.x.

Robinson, S.E., Bohon, W., Kleber, E.J., J Arrowsmith, R., Crosby, C.J., 2017. Applications of high-resolution topography in Earth science education. Geosphere 13, 6. https://doi.org/10.1130/GES01236.1.

Schumm, S.A., Hadley, R.F., 1957. Arroyos and the semi-arid cycle of erosion (Wyoming and New Mexico). Am. J. Sci. 255, 161–174. https://doi.org/10.2475/ajs.255.3.161.

Schürch, P., Densmore, A.L., Rosser, N.J., Lim, M., McArdell, B.W., 2011. Detection of surface change in complex topography using terrestrial laser scanning: application to the Illgraben debris-flow channel. Earth Surf. Process. Landf. 36 (14), 1847–1859. https://doi.org/10.1002/esp.2206.

Shan, Q., Wu, C., Curless, B., Furukawa, Y., Hernandez, C., Seitz, S.M., 2014. Accurate geo-registration by ground-to-aerial image matching. In: 2014 2nd International Conference on 3D Vision, 8–11 Dec. 2014, Tokyo, Japan. https://doi.org/10.1109/3DV.2014.69.

Smith, M.W., Vericat, D., 2015. From experimental plots to experimental landscapes: topography, erosion and deposition in subhumid badlands from structure-from-motion photogrammetry. Earth Surf. Process. Landf. 40 (12), 1656–1671. https://doi.org/10.1002/esp.3747.

Smith, D.E., Zuber, M.T., Neumann, G.A., Lemoine, F.G., 1997. Topography of the Moon from the Clementine lidar. J. Geophys. Res. 102 (E1), 1591–19611.

Smith, D.E., Zuber, M.T., Solomon, S.C., Phillips, R.J., Head, J.W., Garvin, J.B., Banerdt, B.W., Muhleman, D.O., Pettengill, G.H., Neumann, G.A., Lemoine, F.G., Abshire, J.B., Aharonson, O., Brown, D.C., Hauck, S.A., Ivanov, A.B., McGovern, P.J., Zwally, J.H., Duxbury, T.C., 1999. The global topography of Mars and implications for surface evolution. Science 284 (5419), 1495–1503. https://doi.org/10.1126/science.284.5419.1495.

Snavely, N., Seitz, S.M., Szeliski, R., 2006. Photo tourism: exploring image collections in 3D. ACM Trans. Graph. 25 (3), 835–846. https://doi.org/10.1145/1141911.1141964.

Snavely, N., Seitz, S.M., Szeliski, R., 2008. Modeling the world from Internet photo collections. Int. J. Comput. Vis. 80 (2), 189–210. https://doi.org/10.1007/s11263-007-0107-3.

Sofia, G., Bailly, J., Chehata, N., Tarolli, P., Levavesseur, F., 2016. Comparison of Pleiades and LiDAR digital elevation models for terraces detection in farmlands. IEEE J. Sel. Top. Appl. Earth Obs. Remote Sens. 9 (4), 1567–1576. https://doi.org/10.1109/JSTARS.2016.2516900.

Stöcker, C., Eltner, A., Karrasch, P., 2015. Measuring gullies by synergetic application of UAV and close range photogrammetry—a case study from Andalusia, Spain. Catena 132, 1–11. https://doi.org/10.1016/j.catena.2015.04.004.

Stojic, M., Chandler, J.H., Ashmore, P., Luce, J., 1998. The assessment of sediment transport rates by automated digital photogrammetry. Photogramm. Eng. Remote. Sens. 64 (5), 387–395.

Strick, R.J.P., Ashworth, P.J., Sambrook Smith, G.H., Nicholas, A.P., Best, J.L., Lane, S.N., Parsons, D.R., Simpson, C.J., Unsworth, C.A., Dale, J., 2019. Quantification of bedform dynamics and bedload sediment flux in sandy braided rivers from airborne and satellite imagery. Earth Surf. Process. Landf. 44 (4), 953–972. https://doi.org/10.1002/esp.4558.

Sturznegger, M., Stead, D., 2009. Close-range terrestrial digital photogrammetry and terrestrial laser scanning for discontinuity characterization on rock cuts. Eng. Geol. 106 (3–4), 163–182. https://doi.org/10.1016/j.enggeo.2009.03.004.

Tarolli, P., 2014. High-resolution topography for understanding Earth surface processes: opportunities and challenges. Geomorphology 216, 295–312. https://doi.org/10.1016/j.geomorph.2014.03.008.
Tarolli, P., Dalla Fontana, G., 2009. Hillslope-to-valley transition morphology: new opportunities from high resolution DTMs. Geomorphology 113, 47–56. https://doi.org/10.1016/j.geomorph. 2009.02.006.
Tarolli, P., Sofia, G., 2016. Human topographic signatures and derived geomorphic processes across landscapes. Geomorphology 255, 140–161. https://doi.org/10.1016/j.geomorph.2015.12.007.
Tarolli, P., Sofia, G., Dalla Fontana, G., 2012. Geomorphic features extraction from high-resolution topography: landslide crowns and bank erosion. Nat. Hazards 61, 65–83. https://doi.org/10.1007/s11069-010-9695-2.
Tarolli, P., Cao, W., Sofia, G., Evans, D., Ellis, E.C., 2019a. From features to fingerprints: a general diagnostic framework for anthropogenic geomorphology. Prog. Phys. Geogr. Earth Environ. 43, 95–128. https://doi.org/10.1177/0309133318825284.
Tarolli, P., Cavalli, M., Masin, R., 2019b. High-resolution morphologic characterization of conservation agriculture. Catena 172, 846–856. https://doi.org/10.1016/j.catena.2018.08.026.
Trevisani, S., Cavalli, M., Marchi, L., 2010. Reading the bed morphology of a mountain stream: a geomorphometric study on high-resolution topographic data. Hydrol. Earth Syst. Sci. 14, 393–405. https://doi.org/10.5194/hess-14-393-2010.
Triggs, B., McLauchlan, P.F., Hartley, R.I., Fitzgibbon, A.W., 2000. Bundle adjustment—a modern synthesis. In: Triggs, B., Zisserman, A., Szeliski, R. (Eds.), Vision Algorithms '99, LNCS 1883. Springer-Verlag, Berlin Heidelberg, pp. 298–372.
Tuckfield, C.G., 1964. Gully erosion in the New Forest, Hampshire. Am. J. Sci. 262, 795–807. https://doi.org/10.2475/ajs.262.6.795.
Ullman, S., 1979. The interpretation of structure from motion. Proc. R. Soc. Lond. B 203 (1153), 405–426. https://doi.org/10.1098/rspb.1979.0006.
Vanmaercke, M., Poesen, J., Van mele, B., Demuzere, M., Bruynseels, A., Golosov, V., Rodrigues Bezerra, J.S., Bolysov, S., Dvinskih, A., Frankl, A., Fuseina, Y., Teixeira Guerra, A.J., Haregeweyn, N., Ioniță, I., Makanzu Imwangana, F., Moeyersons, J., Moshe, I., Nazari Samani, A., Niacșu, L., Nyssen, J., Otsuki, O., Rădoane, M., Rysin, I., Ryzhov, Y.V., Yermolaev, O., 2016. How fast do gully headcuts retreat? Earth Sci. Rev. 154, 336–355. https://doi.org/10.1016/j.earscirev.2016.01.009.
Ventura, G., Vilardo, G., Terranova, C., Bellucci Sessa, E., 2011. Tracking and evolution of complex active landslides by multi-temporal airborne LiDAR data: the Montaguto landslide (Southern Italy). Remote Sens. Environ. 115 (12), 3237–3248. https://doi.org/10.1016/j.rse.2011.07.007.
Viles, H., 2016. Technology and geomorphology: are improvements in data collection techniques transforming geomorphic science? Geomorphology 270, 121–133. https://doi.org/10.1016/j.geomorph.2016.07.011.
Vinci, A., Brigante, R., Todisco, F., Mannocchi, F., Radicioni, F., 2015. Measuring rill erosion by laser scanning. Catena 124, 97–108. https://doi.org/10.1016/j.catena.2014.09.003.
Wang, R., Zhang, S., Pu, L., Yang, J., Yang, C., Chen, J., Guan, C., Wang, Q., Chen, D., Fu, B., Sang, X., 2016. Gully erosion mapping and monitoring at multiple scales based on multi-source remote sensing data of the Sancha River Catchment, Northeast China. ISPRS Int. J. Geo-Inf. 5 (200), 1–17. https://doi.org/10.3390/ijgi5110200.
Wehr, A., Lohr, U., 1999. Airborne laser scanning—an introduction and overview. ISPRS J. Photogramm. Remote Sens. 54 (2–3), 68–82. https://doi.org/10.1016/S0924-2716(99)00011-8.
Wells, R.R., Momm, H.G., Castillo, C., 2017. Quantifying uncertainty in high-resolution remotely sensed topographic surveys for ephemeral gully channel monitoring. Earth Surf. Dyn. 5, 347–367. https://doi.org/10.5194/esurf-5-347-2017.
Westoby, M.J., Brasington, J., Glasser, N.F., Hambrey, M.J., Reynolds, J.M., 2012. 'Structure-from-Motion' photogrammetry: a low-cost, effective tool for geoscience applications. Geomorphology 179, 300–314. https://doi.org/10.1016/j.geomorph.2012.08.021.
Wheaton, J.M., 2008. Uncertainty in Morphological Sediment Budgeting of Rivers. Unpublished PhD, University of Southampton, Southampton. 412 pp http://www.joewheaton.org/Home/research/projects-1/phdthesis.
Wheaton, J.M., Brasington, J., Darby, S.E., Sear, D., 2010. Accounting for uncertainty in DEMs from repeat topographic surveys: improved sediment budgets. Earth Surf. Process. Landf. 35 (2), 136–156. https://doi.org/10.1002/esp.1886.
Wu, C., 2013. Towards linear-time incremental structure from motion. In: 2013 International Conference on 3D Vision (3DV 2013), Proceedings of a Meeting held 29 June–1 July 2013, Seattle, Washington, USA. vol. 127. , pp. 1–8.

Wu, C., 2015. P3.5P: pose estimation with unknown focal length. In: 2015 IEEE Conference on Computer Vision and Pattern Recognition (CVPR), 7–12 June 2015, Boston, MA, USA. https://doi.org/10.1109/CVPR.2015.7298858.
Wu, C., Agarwal, S., Curless, B., Seitz, S.M., 2011. Multicore bundle adjustment. In: IEEE Computer Vision and Pattern Recognition (CVPR), Colorado Springs. https://grail.cs.washington.edu/projects/mcba/poster-mcba.pdf.
Wu, H., Zu, X., Zheng, F., Qin, C., He, X., 2017. Gully morphological characteristics in the loess hilly-gully region based on 3D laser scanning technique. Earth Surf. Process. Landf. 43 (8), 1701–1710. https://doi.org/10.1002/esp.4332.
Xiang, J., Chen, J., Sofia, G., Tian, Y., Tarolli, P., 2018. Open-pit mine geomorphic changes analysis using multi-temporal UAV survey. Environ. Earth Sci.. 77. https://doi.org/10.1007/s12665-018-7383-9.
Xu, Y., Yue, D., He, P., 2017. Point cloud segmentation of gully based on characteristic difference using airborne LiDAR data. ISPRS Arch. XLII-2/W7, 307–311. https://doi.org/10.5194/isprs-archives-XLII-2-W7-307-2017.
Zheng, E., Wu, C., 2015. Structure from motion using structure-less resection. In: 2015 IEEE International Conference on Computer Vision (ICCV), 7–13 December 2015, Santiago, Chile. https://doi.org/10.1109/ICCV.2015.240.

Further reading

Fryer, J.G., Brown, D.C., 1986. Lens distortion for close-range photogrammetry. Photogram. Eng. Remote Sens. 52, 51–58.
Lohr, U., 1998. Digital elevation models by laser scanning. Photogramm. Rec. 16 (91), 105–109. https://doi.org/10.1111/0031-868X.00117.
Sofia, G., Mariniello, F., Tarolli, P., 2014. A new landscape metric for the identification of terraced sites: the Slope Local Length of Auto-Correlation (SLLAC). ISPRS J. Photogramm. Remote Sens. 96, 123–133. https://doi.org/10.1016/j.isprsjprs.2014.06.018.
Tarolli, P., Calligaro, S., Cazorzi, F., Dalla Fontana, G., 2013. Recognition of surface flow processes influenced by roads and trails in mountain areas using high-resolution topography. Eur. J. Remote Sens. 46, 176–197. https://doi.org/10.5721/EuJRS20134610.0.1029/2017EO069637.
Tarolli, P., Sofia, G., Calligaro, S., Prosdocimi, M., Preti, F., Dalla Fontana, G., 2015. Vineyards in terraced landscapes: new opportunities from lidar data. Land Degrad. Dev. 26, 92–102. https://doi.org/10.1002/ldr.2311.